SCIENCE CHINA
Chemistry

• REVIEWS •
· SPECIAL ISSUE · Organic Electronics and Photonics

April 2017 Vol.60 No.4: 472–489
doi: 10.1007/s11426-016-9023-5

Transition metal oxides as hole-transporting materials in organic semiconductor and hybrid perovskite based solar cells

Pingli Qin[1,2,4], Qin He[3], Dan Ouyang[5], Guojia Fang[4], Wallace C.H. Choy[5] & Gang Li[1*]

[1]*Department of Electronic and Information Engineering, The Hong Kong Polytechnic University, Hong Hum, Kowloon, Hong Kong SAR, China*
[2]*School of Science, Wuhan Institute of Technology, Wuhan 430073, China*
[3]*College of Post and Telecommunications, Wuhan Institute of Technology, Wuhan 430073, China*
[4]*Key Laboratory of Artificial Micro- and Nano-structures of the Ministry of Education, School of Physics and Technology, Wuhan University, Wuhan 430072, China*
[5]*Department of Electrical and Electronic Engineering, The University of Hong Kong, Hong Kong SAR, China*

Received December 16, 2016; accepted February 20, 2017; published online March 14, 2017

Organic polymer solar cells (OSCs) and organic-inorganic hybrid perovskite solar cells (PSCs) have achieved notable progress over the past several years. A central topic in these fields is exploring electronically efficient, stable and effective hole-transporting layer (HTL) materials. The goal is to enhance hole-collection ability, reduce charge recombination, increase built-in voltage, and hence improve the performance as well as the device stability. Transition metal oxides (TMOs) semiconductors such as NiO_x, CuO_x, CrO_x, MoO_x, WO_3, and V_2O_5, have been widely used as HTLs in OSCs. These TMOs are naturally adopted into PSC as HTLs and shows their importance. There are similarities, and also differences in applying TMOs in these two types of main solution processed solar cells. This concise review is on the recent developments of transition metal oxide HTL in OSCs and PSCs. The paper starts from the discussion of the cation valence and electronic structure of the transition metal oxide materials, followed by analyzing the structure-property relationships of these HTLs, which we attempt to give a systematic introduction about the influences of their cation valence, electronic structure, work function and film property on device performance.

hole-transporting layer, transition metal oxide, perovskite solar cell, organic solar cell

Citation: Qin P, He Q, Ouyang D, Fang G, Choy WCH, Li G. Transition metal oxides as hole-transporting materials in organic semiconductor and hybrid perovskite based solar cells. *Sci China Chem*, 2017, 60: 472–489, doi: 10.1007/s11426-016-9023-5

1 Introduction

Solar energy is the most promising clean, renewable, abundant and sustainable source of energy that is expected to make considerable contributions to solving the global renewable-energy challenge. Solution processed organic solar cells (OSCs) based on polymers and small molecules, have attracted much attention in the past two decades due to their potential as low-cost, light weight, and large-area flexible photovoltaic devices [1–5]. The power conversion efficiencies (PCEs) of the state-of-the-art OSCs has reached certified 11.7% [6], resulting from the progress in new materials, device engineering, device physics, etc. [7–10]. More recently, solar cells based on organic-inorganic hybrid perovskites, such as methyl ammonium lead iodide ($CH_3NH_3PbI_3$), have achieved an unexpected breakthrough and rapid evolution with PCEs exceeding 22% after an impressive short research and development time [11–17]. However, there are still many issues that restrict the commercialization of OSCs and PSCs from lab-scale to large area fabrication, including high throughput, low cost, easy fabrication, scalability, and low

*Corresponding author (email: gang.w.li@polyu.edu.hk)

temperature processing technology, low toxicity and long term stability. Previous reports and reviews mainly concentrated on the design of device structures, development and controlling the morphology of each function layer materials, modification of different interfaces, and degradation mechanism of devices [13,18–26]. In this review, we will focus the recent progress on one key component in the organic and organic-inorganic hybrid perovskite solar cells—hole transporting layer (HTL).

The pristine photoactive layer (PAL) in organic-inorganic hybrid perovskite solar cells is very delicate—the degradation of devices would be accelerated as exposed to ambient environment [27–30]. It is known that the perovskite materials are extremely sensitive to moisture [31], and can easily degrade to form the intermediate hydrated phases and iodine/iodide with ambient air exposure [32–37]. Proper interfacial layers have been shown to significantly (not ultimately) slow down the degradation process.

By function, HTL materials extract photo-generated carrier (hole) from PAL to anode. Hole-mobility is typically lower than that of electron in OSCs and PSCs [38–40]. It is thus very important to have efficient hole transport in HTL and eliminate energy barriers at PAL/HTL & HTL/Anode interfaces, in ordert to achieve high device efficiency. In principle, an ideal HTL for highly efficient OSCs and PSCs needs to meet the following requirements: (1) wide band gap; (2) proper energy level matched with that of PAL; (3) high mobility; (4) low-temperature solution processability; (5) suitable surface energy for photo-active layer crystal growth; (6) effective suppression of diffusion between the electrode material and PAL; (7) withstand organic solvent; (8) chemically inert—not react with adjacent materials [41].

To date, there are many studies focused on HTL materials on solution processed polymer and perovskite solar cells, as well as their influence on the solar cell performance [13,15,25,26,30,42]. In the two types of solution processed solar cells, polymer or small molecule HTLs have often been used, such as poly(3,4-ethylene dioxythiophene):poly(4-styrenesulfonate) (PEDOT:PSS), poly [bis (4-phenyl) (2,4,6-trimethylphenyl)-amine] (PTAA), and 2,2′,7,7′-tetrakis (*N*,*N*′-di-*p*-methoxyphenylamine)-9,9′-spirobifluorene (spiro-OMeTAD) as HTLs [43–47]. However, the onerous synthesis, water absorbing property, and the low charge-carrier mobility of organics significantly hamper their applications [26,48–50]. Specially, Li^+ doping in spiro-OMeTAD can result in the poor stability of PSCs. Transition metal oxide (TMO) HTL materials, including NiO, CuO_x, CrO_x, MoO_3, V_2O_5, and WO_3 [51–57], have been utilized as HTLs in OSCs owing to their wide band-gap, good chemical (or thermal) stability, high work function, and good hole-transport properties. Numerous studies on corresponding OSC devices with TMO showed comparable/better PCE and much better stability than the devices with organic HTL. The TMO HTL materials also attracts great attention in PSC, and we will review the progress in this article as well.

2 TMO HTL materials—cation valence and electronic structure

Transition metals are elements with partially filled d orbitals, with one to nine electrons in the outer shell. In a solid, these d orbitals form relatively narrow d bands. For example, in the case of vanadium, the next higher 4s band is substantially broader and overlaps with the entire d band, resulting in an occupied 4s band and metallic conductivity of the transition metal. In TMOs, the 2p orbitals, which originate from the oxygen anion, are completely filled and form the valence band of the material. In the case of V_2O_5 the metallic cations form the 3d band, which is partially filled. Because of the bonding/anti-bonding splitting between the 2p and 4s bands, the cationic 4s band is several eVs above the 3d band and therefore completely empty at zero temperature. The cation 3d band (conduction bands) is therefore responsible for the electronic properties of the material [58]. The applications of TMOs to OSC and PSC's HTLs arise from those semiconducting properties.

2.1 p-Type transition metal oxides as HTL materials

2.1.1 Nickel oxide

Nickel oxide is a wide band-gap (direct band-gap, E_g ~3.7 eV), transparent p-type semiconductor with weak absorption bands due to d-d transitions of $3d^8$ electron configuration in the visible region [59–63]. X-ray photoelectron spectroscopy (XPS) of the solution-derived NiO_x films shows the XPS spectrum for the Ni $2P_{3/2}$ state, which can be separated into three peaks. The peak centered at a binding energy of 853.7 eV corresponds to Ni^{2+} in the standard Ni–O octahedral bonding configuration, the broad peak centered at 860.8 eV has been ascribed to a shakeup process in the NiO_x structure, and the peak centered at 855.5 eV has been ascribed to the Ni^{2+} vacancy-induced Ni^{3+} ion [64–66] or nickel hydroxides and oxyhydroxides (Figure 1(a)) [59,64,65]. It has been reported that there was a tinny different peak for Ni^{3+} state in the XPS spectrum. The peak of Ni^{3+} stated in NiOOH is located at 856.3 eV, while the peak of Ni^{3+} state in Ni_2O_3 appears at 855.0 eV [67]. Moreover, the XPS spectrum for the O 1s state can be separated into two distinct peaks. The peak centered at 529.2 eV confirms the Ni–O octahedral bonding in NiO, and the peak at 531.0 eV is the indication of nickel hydroxides and oxyhydroxides, including defective nickel oxide with hydroxyl groups adsorbed on the surface (Figure 1(b)) [68,69]. XPS spectra showing different peaks for the O 1s in NiOOH (at 531.1 eV) and Ni_2O_3 (at 530.8 eV) have been reported [67]. It was also concluded that the

annealing temperature could affect the composition of NiO_x film according to the change of the dominant peak in XPS spectrum.

The ultraviolet and inverse photoemission spectroscopies (UPS, IPES) of the density of states near the valence and conduction band edges of NiO_x are shown in Figure 2(a, b), and the summary of the UPS and IPES results in the form of energy level positions is given in Figure 2(c). The photoemission cutoff given in Figure 1(a) indicates NiO_x has a 4.8 eV work function (WF) and 5.2 eV valence band ionization energy (IE). Another type of post-treatment-free NiO_x gives the Fermi level (E_F) of 5.25 eV with a conduction band (CB) of 1.85 eV and a valence band (VB) of 5.01 eV. It is also illustrated that the E_F of the film shifted to 5.13 eV, accompanied with CB of 1.76 eV and VB of 5.40 eV after 150 °C annealing treatment [67]. With O_2-plasma treatment, the WF and IE change to 5.3 and 5.7 eV respectively. This indicates that there are 0.5 eV downward shifts for WF and IE with respect to the vacuum level of NiO_x film. In contrast, the O_2-plasma treatment does not affect the electron affinity (EA), which remains constant at 2.1 eV. The valence band edge is ca. 0.4 eV below the Fermi level (shown in Figure 1(b)), indicating that NiO_x is a p-type material which is likely doped upon O_2-plasma treatment. From the energy diagram (Figure 2(c)), we can infer that NiO_x result in a high performance HTL due to better contact between a high WF O_2-plasma treated NiO_x and a high IE donor materials, better electron blocking ability of 2.1 eV conduction band edge, and wider band gap (3.6 eV when O_2-plasma treated) [70].

2.1.2 Copper oxide

Copper oxide is another p-type TMO material. CuO has a high concentration of Cu vacancies and stable defects under O-rich conditions [71], and Cu_2O has over 100 $cm^2/(V\ s)$ hole-mobility, and high stability within certain temperature and oxygen pressure range [72,73]. The Cu $2p_{3/2}$

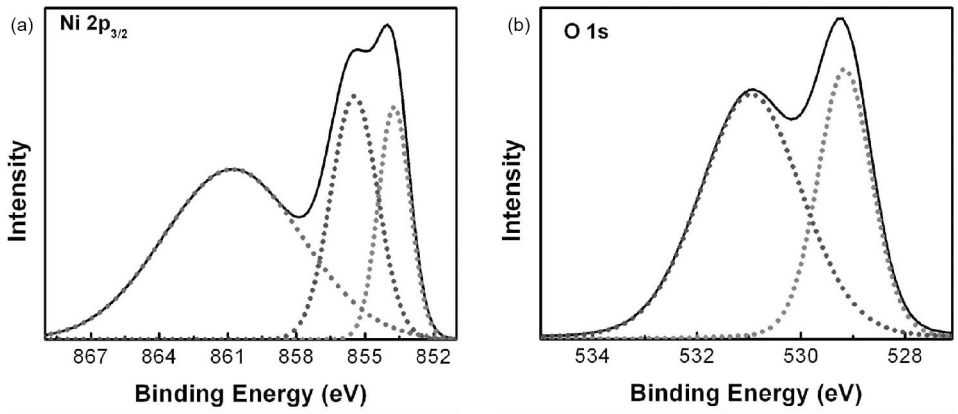

Figure 1 (a) High resolution Ni $2P_{3/2}$ XPS acquisition for NiO. The spectrum shows three contributions: one from Ni^{2+} in the octahedral NiO configuration at low binding energy, one from hydroxylated or defective NiO at an intermediate binding energy, and one from a shake-up process in the NiO lattice at the highest binding energy. (b) High resolution O 1s XPS acquisition for NiO. The spectrum shows two contributions: one from O^{2-} in the octahedral NiO configuration at low binding energy and one from hydroxylated or defective NiO at a higher binding energy [59].

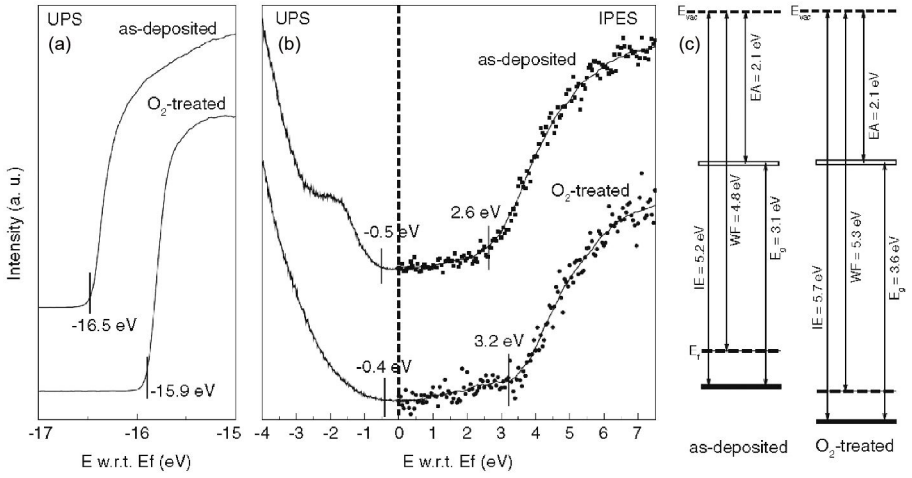

Figure 2 UPS and IPES measurements of the density of states near the valence band edge and conduction band and resulting band energies. (a) UPS spectra (He I) of the photoemission cut-off showing an increase in WF after O_2-plasma treatment of the NiO_x; (b) combined UPS and IPES spectra of the NiO_x near the valence and conduction band edge; (c) energy level diagrams of NiO_x before and after O_2-plasma treatment [70].

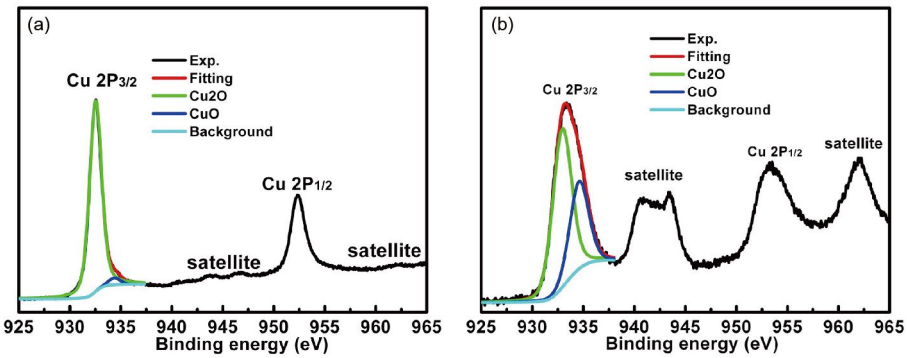

Figure 3 The Cu $2P_{3/2}$ core level peaks of (a) the as-deposited and (b) UVO-treated CuO_x films (color online).

peak for the CuO_x thin film with is centered at a binding energy of ~932.5 eV, and the 19.8 eV splitting feature between the Cu $2p_{1/2}$ and $2p_{3/2}$ is the same as that of Cu_2O [74]. Two smaller peaks near 943 and 946 eV are shown in Figure 3(a), which indicate that CuO phase is formed in the sample. On the base of asymmetric peak Cu $2p_{3/2}$ with fitted Gaussian-Lorentzian curves, it is found that ~97.2% Cu_2O (932.5 eV) and ~2.8% CuO (934.4 eV) exist in CuO_x thin film. With UV-ozone treatment, the intensity ratio of Cu^{2+}/Cu^{1+} in the ultraviolet ozone (UVO)-treated CuO_x film increases apparently (Figure 3(b)). Broad satellite peaks near 940–943 eV originate from the CuO phase, which is a characteristic of materials having a d^9 configuration in the ground state [75]. This is shown that the as-deposited CuO_x film is further oxidized. For the p-type metal oxide semiconductors, a considerable concentration of the free holes exist in the valence band. The concentration of the free holes is mainly determined by the metal deficit or excess oxygen concentration within the crystallite sites of the materials, which is attributed to the deviation from the stoichiometric composition of the components [71]. Herein, the UV-ozone treatment increases oxygen concentration and the content of Cu^{2+} ions in the CuO film, thus tunes its WF from 4.96 eV to 5.30 eV (Figure 4). The corresponding valence band maximums (VBM) associated with IE of the as-deposited and UVO-treated CuO_x films appear at 0.90 and 0.61 eV, respectively, with respect to the Fermi level. Thus, the valence band maximums of the as-deposited and UVO-treated CuO_x films are estimated to be 5.86 and 5.91 eV, respectively. Compared to that of the as-deposited CuO film, the Fermi level of UVO treated CuO film shifts to the valence band, indicating an enhanced p-type semiconductor characteristic of the CuO_x film after UV-ozone treatment. However, it is not the optimal HTLs for inverted-PSCs because of the narrow band gaps of CuO (1.3–2.0 eV) and Cu_2O (2.1–2.3 eV) [71–73,76,77].

2.2 n-Type TMO—chromium oxide, molybdenum oxide, tungsten oxide and vanadium oxide

Since molybdenum (Mo), tungsten (W) and chromium (Cr) belong to the same group transition-metals, the corresponding TMOs have a similar nature. CrO_x film is composed of Cr^{3+}, Cr^{4+} and Cr^{6+} oxidation states fabricated by radio frequency sputtering method (Figure 5(a)). MoO_3 and WO_3 films formed with the multivalent cations [78,79] are shown in Figure 5(b, c). Similarly, V^{5+} and V^{4+} oxidation states are formed in V_2O_5 film (shown in Figure 5(d)) [80–82].

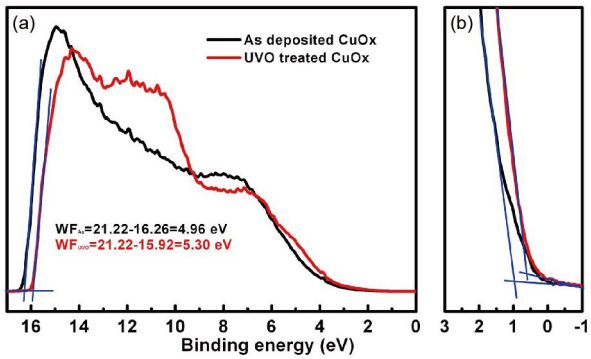

Figure 4 UPS spectra of the as-deposited and UVO-treated CuO_x films. The full UPS spectra using He I radiation (a), and the valence-band region (b) are included (color online).

Early reports presented TMOs such as Cr_2O_3, MoO_3, WO_3, and V_2O_5 as conducting p-type materials [53,54,83,84] because the point defects of excess oxygen ions and metal vacancies are the predominating defects [37,53,80–82,85–88]. For instance, the WF, EA and IE of MoO_3 often are quoted in literature to be on the order of 5.2, 2.3, and 5.3–5.4 eV, respectively [89–95]. However, it was recently demonstrated with direct and inverse photoemission spectroscopy measurements that Cr_2O_3, MoO_3, WO_3, and V_2O_5 are n-type materials exhibiting very deep lying electronic states (Figure 6) [37,58,91,93,95]. Ultrahigh vacuum (UHV) MoO_3 prepared by evaporation possesses a 6.86 eV Fermi level, a 6.70 eV EA and 9.68 eV IE. Evaporated transition metal oxides—WO_3 and V_2O_5 with even higher WFs of ca. 6.7 and 7.0 eV, respectively (Figure 6(b)) [80]. These show that they are n-type materials [79]. The fact that they function as HTL may be associated with the multivalence state of metal cation. Nevertheless, the existence of multivalence states leads to defects

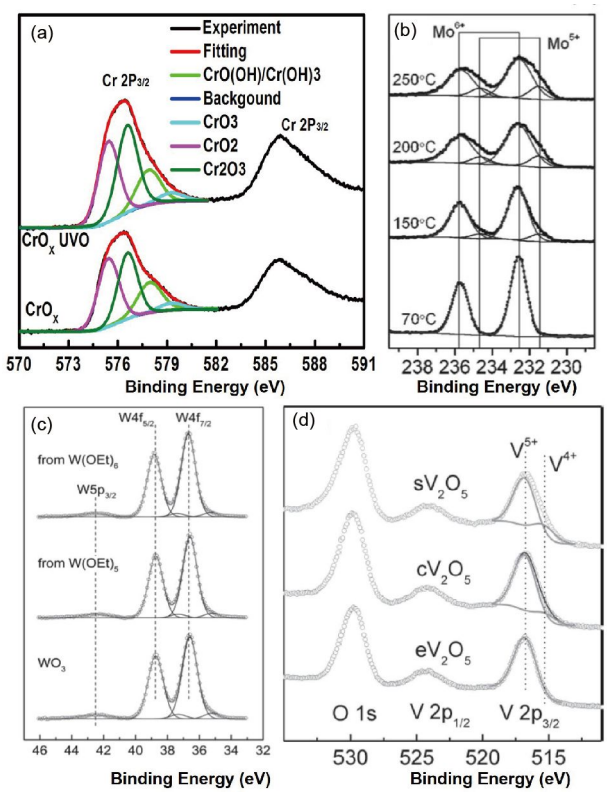

Figure 5 XPS spectra of (a) Cr 2p, (b) Mo 3d, (c) V 2p, and (d) W 4f core level peaks observed for molybdenum oxide thin films [37,80–82] (color online).

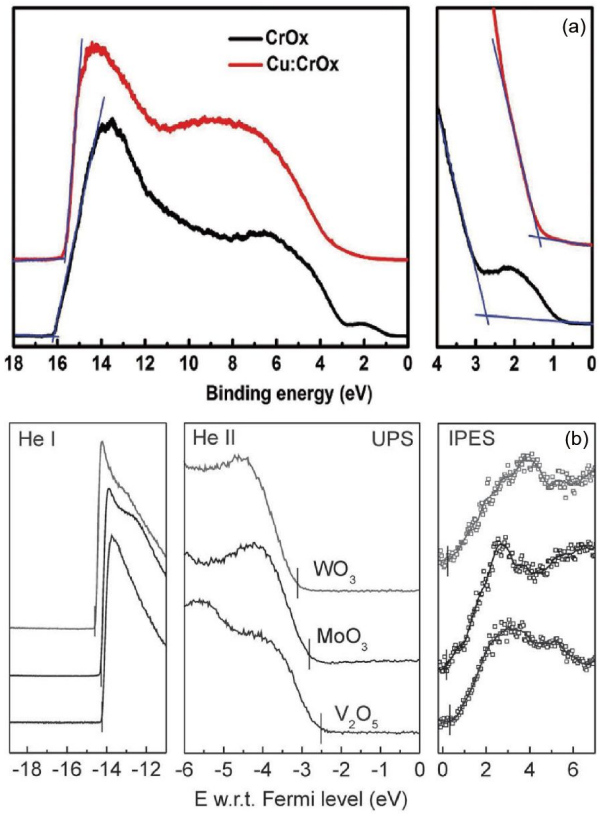

Figure 6 (a) UPS spectra of CrO_x and Cu:CrO_x films with UVO treatment. The full UPS spectra using He I radiation (left) and the valence-band region (right) are included. (b) UPS and IPES spectra of vacuum grown MoO_3, V_2O_5 and WO_3. The left panel shows the photoemission onset, the middle panel shows the density of filled states near the valence band (VB) edge, and the right panel shows the density of empty states near the conduction band (CB) edge. The reference is the Fermi level, measured separately on a metallic electrode. The tick marks denote the onset position, the top of the VB, and the bottom of the conduction band [37,58,91,93,110] (color online).

in these metal oxide films (Figure 7), especially on the surface [78,79,96]. These defects could have very strong adsorption properties of water and oxygen, which are not beneficial to the stability of OSCs and PSCs. Therefore, many research groups have tried to improve the hole-mobility and stability of inorganic oxide HTL from every aspect, and various fabrication methods and engineering have been employed to prepare the HTL [97–110]. It is worth mentioning that the very different workfunction from UHV and normal high vacuum evaporation is due to the existence of oxygen in the evaporation case.

3 TMO as HTL in OSCs and inverted planar PSCs

The basic polymer OSC has a sandwiched structure with a bulk heterojunction (BHJ) blend of an electron-donating conjugated polymer and an electron-accepting fullerene or non-fullerene acceptor as a PAL between two electrodes, one or both are transparent (Figure 8(a)). In such a device the absorption of a photon in the PAL excites an electron from the highest occupied molecular orbital (HOMO) to the lowest unoccupied molecular orbital (LUMO) in molecules which create exciton. The exciton dissociation at donor/acceptor interface, driven by the energy level difference between the two

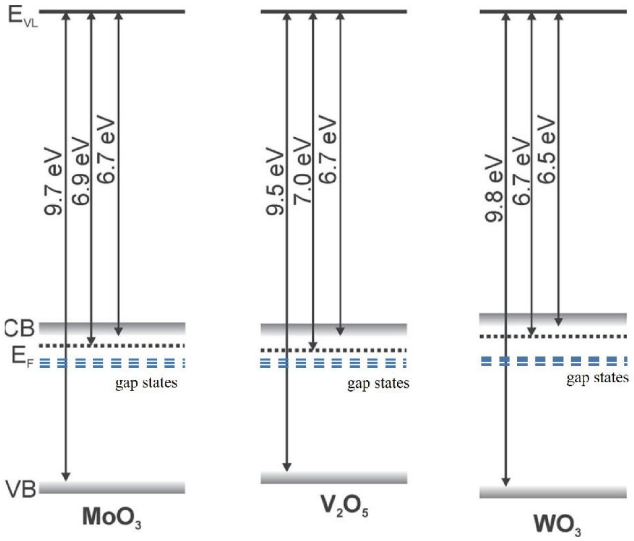

Figure 7 CB minimum and VB maximum with respect to the vacuum level (E_{VL}) for MoO_3, V_2O_5 and WO_3, deduced from the UPS and IPES measurements depicted in Figure 6. The ionization energy, work function and electron affinity are indicated in each case (color online).

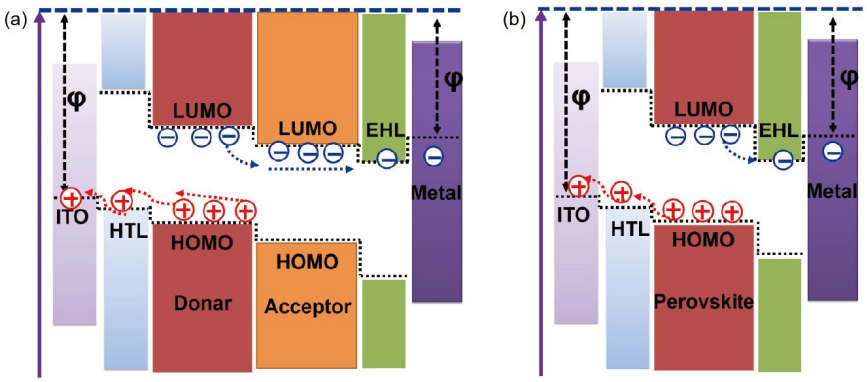

Figure 8 Schematic illustration of energy levels of each layer and charge transfer in (a) OSC and (b) inverted planar PSC (color online).

materials is a result of ultrafast electron transfer from the donor to the acceptor molecules. The separated free carriers are then (ideally) transported to their respective electrodes under the influence of the internal electric field to generate the photo-voltage and photocurrent [111]. For inverted planar PSCs, perovskite photoactive materials are ambipolar charge-conductors, therefore, free negative and positive charge carriers generated are transported through the perovskite to the interface between itself and HTL, or electron transfer layer. Under matched energy levels of each layer of the device (Figure 8(b)), the HOMO of HTL is slightly higher than that of perovskite, and the holes at the interface between HTL and perovskite can be extracted into HTL and then fast transferred to anode [112]. Generally, HTL in conventional OSC and inverted PSC is naturally exhibited to transport holes and block electrons. The large gap between the LUMO of HTL and that of PAL can effectively block the electron transferring to anode. The matched energy level avoids the depletion of holes within the PAL and the accumulation of holes at interface, reducing charge recombination possibility, and ultimately helping high PCE.

Semiconducting TMOs, such as NiO_x, CuO_x, CrO_x, MoO_3, V_2O_5, and WO_3 [51–56], have high chemical (or thermal) stability, wide band-gap, deep valence band position (or gap states, Figure 7), and low conduction band edges (or potential barrier) to effectively block electron transferring to anode, high hole-transport property. These make them promising candidates for PV applications, since the early work of using thermal evaporated MoO_3, V_2O_5 film as HTL by Shrotriya *et al*. [56] a decade ago. Table 1 is a summary of polymer OSCs using TMO as HTLs.

3.1 Nickel oxide HTL

Among the transition metal semiconductor HTLs, NiO_x is widely studied at present. NiO is a cubic wide band gap p-type semiconductor and usually hybrid with Ni^{3+}, which is also presented as NiO_x [62]. The p-type conductivity of NiO_x originates from two positively charged holes which accompany each Ni^{2+} vacancy in the lattice for charge neutrality. These holes are quasi-localized on Ni^{2+} ions near the vacancy in the lattice, generating two Ni^{3+} ions for each Ni^{2+} vacancy. It has high transmittance with a wide band-gap of ca. 3.7 eV and high work function of ca. 5.2 eV. The valence band edge of NiO_x is well-aligned to the HOMO levels of many p-type conjugated polymers for photovoltaics [59]. The electronic structure of NiO_x offers attractive hole-transporting and electron-blocking properties, making NiO_x thin films good for HTL applications.

Irwin *et al*. [51] demonstrated an enhancement in OSC performance with a NiO HTL deposited via pulsed laser deposition (PLD). An open-circuit voltage (V_{oc}) of 0.638 V, a fill factor (FF) of 0.693, a short-circuit current density (J_{sc}) of 11.3 mA/cm^2, and a corresponding PCE of 5.16% are obtained (Table 1) in P3HT:PCBM solar cell—a record that time. Magnetron sputtering then became a commonly method for preparing NiO_x film [62,118–120]. It is found that the NiO_x film deposited at room temperature can possess the lowest electrical resistivity [62], which is beneficial to improve the hole transport and collection [119]. The low-temperature sputtering process showed good compatibility in flexible devices. However, both PLD and sputtering need the vacuum environment, and increase the cost of OSC, which is not benefit for the commercialization of OSCs and PSCs from lab-scale to large area fabrication.

In order to reduce the cost of TMO HTL, solution-processed NiO_x was also reported for OSC, resulting in a remarkable PCE of 7.8% [59]. However, the high annealing temperature (≥250 °C) [118] required to convert the nickel precursors into the NiO_x thin films, brings in new challenge, as it is not compatible with flexible substrates. Gao's group [113] exploited a low temperature approach (chemistry combustion method) to fabricate high quality NiO_x HTLs with the processing temperature as low as 175 °C, and the solution-processed OSC devices showed a high PCE of 6.42%.

Through the research on NiO film by PLD and solution deposition, it was found that nickel hydroxides and oxyhydroxides, including defective nickel oxide with hydroxyl groups adsorbed on the surface, affect the surface properties of NiO_x.

Table 1 Performance parameters of OSCs with TMO films as interface layers

Structure of device [a)]	HTL prepared method and annealing temperature	V_{oc} (V)	J_{sc} (mA/cm^2)	FF (%)	PCE (%)	Ref.
ITO/NiO (10 nm)/ P3HT:$PC_{61}BM$/Ca/Al	Pulsed-laser deposition	0.638	11.3	69.3	5.16	[51]
ITO/NiO_x/PCDTBT:$PC_{70}BM$/Ca/Al	Solution deposition, 300 °C	0.879	11.5	65.0	6.7	[70]
ITO/NiO(5 nm)/pDTG-TPD:$PC_{71}BM$/LiF/Al	Sol-gel deposition, 275 °C	0.82	13.9	68.4	7.8	[59]
ITO/NiO/TQ1:$PC_{71}BM$/Ca/Al	Chemistry combustion, 175 °C	0.87	10.50	70.0	6.42	[113]
ITO/CuO_x/PCDTBT:$PC_{71}BM$/Ca/Al	Sol-gel deposition, 60 °C	0.89	10.58	68.4	6.44	[71]
ITO/CuO_x/PBDTTT-C:$PC_{61}BM$/Ca/Al	Solution deposition, 80 °C	0.71	16.86	59.7	7.14	[52]
ITO/CuO_x/P3HT:ICBA/Ca/Al	Solution deposition, 80 °C	0.86	10.27	71.3	6.29	[52]
ITO/CuO_x/P3HT:$PC_{61}BM$/Ca/Al	Solution deposition, 80 °C	0.59	9.11	68.9	3.70	[52]
FTO/CrO_x (10 nm)/P3HT:$PC_{60}BM$/Al	reactive sputtering, 200 °C	0.54	10.97	55.6	3.28	[53]
ITO/CrO_x/P3HT:ICBA/Ca/Al	UVO treat *in situ*, room temperature	0.87	10.74	70.3	6.55	[114]
ITO/MoO_x/P3HT: $PC_{61}BM$/Al	Solution deposition, 70 °C	0.59	9.5	68	3.8	[81]
ITO/MoO_x/PCDTBT:$PC_{70}BM$/ TiO_x/Al	Thermal evaporation	0.89	10.88	67.2	6.50	[115]
ITO/S-MoO_x/P3HT:$PC_{61}BM$/Al	Sputtering method, 150 °C	0.630	10.05	58.3	3.69	[54]
ITO/MoO_3/MoS_2/P3HT:$PC_{61}BM$/Al	UVO treat *in situ*, room temperature	0.627	9.90	67.1	4.15	[55]
ITO/WO_3/Si-PCPDTBT:$PC_{70}BM$/ Ca/Ag	Solution deposition, 80 °C	0.616	12.8	60.4	4.8	[116]
ITO/ZnO/α-PTPTBT:$PC_{61}BM$/ VO_x/Ag	Solution deposition, room temperature	0.82	11.6	0.53	5.0	[117]

a) P3HT: poly(3-hexylthiophene); $PC_{71/70/61}BM$: [6,6]-phenyl $C_{71/70/61}$-butyric acid methyl ester; PCDTBT:poly(*N*-9′-heptadecanyl-2,7-carbazole-alt-5,5-(4′,7′-di-2-thienyl-2′,1′,3′-benzothidiazole); pDTG-TPD: poly-dithienogermole-thienopyrrolodione; TQ1: poly[2,3-bis-(3-octyloxyphenyl)quinoxaline-5,8-diyl-alt-thiophene-2,5-diyl]; PBDTTT-C:poly(4,8-bis-alkyloxybenzo (1,2-b:4,5-b′)dithiophene-2,6-diyl-alt-(alkyl thieno(3,4-b)thiophene-2-carboxylate)-2,6-diyl); ICBA: indene-C60-bisadduct; Si-PCPDTBT: poly[(4,4′-bis(2-ethylhexyl) dithieno[3,2-b:2′,3′-d]silole)-2,6-diyl-alt-(4,7-bis(2-thienyl)-2,1,3-benzothiadiazole)-5,50-diyl]; α-PTPTBT: poly(thiophene-phenylene-thiophene)-(2,1,3-benzothiadiazole).

Widjonarko's group [121] reported that the presence of NiOOH adsorbate on NiO film tends to increase after O_2 plasma treatment, and the polar nature of NiOOH presumably increases the surface dipole. Moreover, they noted a peak associated to stoichiometric NiO shifts to slightly lower binding energy upon oxygen plasma cleaning, which suggests the formation of unstable non-stoichiometric surface species. Although they found no correlation between this observation and the surface energy data, it is consistent with the observation that the advantageous properties induced by the plasma treatment (improved wetting, increased work-function, etc.) are temporary. Chen *et al*. [122] have treated ultrathin metal Ni films by *in-situ* O_2 plasma to obtain NiO_x HTL on the substrate of aluminum-doped zinc oxide (AZO), and form the NiO_x/Ni/AZO electrode structure, which increases the stability of the underlying AZO and raises the work function to favor injection and collection of charges. This also acts as a protective layer for the underlying AZO.

The research achievement of NiO in OSC stimulate many activities in new field. In 2013, Snaith *et al*. [123] reported that NiO_x was prepared by calcining precursor film of nickel acetate tetrahydrate and monoethanolamine for the HTL of PSCs, but rather poor PCE (<0.1%) was obtained. Subsequently, Chen *et al*. [63] reported an enhancement in PSC performance with a NiO HTL deposited via solution deposition, and obtained a remarkable PCE of 7.8%. Specially, they inserted a layer of mesoscopic NiO_x nanocrystal (NiO_{nc}) between NiO_x and perovskite layer, which acted as a scaffold for sufficient loading of perovskite material to bring a better morphological formation of perovskite atop it. They claim this helps hole-transfer at the NiO_{nc}/perovskite interface, which result in an improved PCE of 9.51% (Figure 9) [124,125]. Many groups were attracted to prepare NiO_x film as the HTL of PSCs [63,125–128]. Bian's group [126] used a solution method to prepare NiO_x film on ITO substrate as the HTL of PSC, and the corresponding PCE achieved is 13.6% in device with structure of ITO/NiO_x/$CH_3NH_3PbI_3$/C60/BCP/Ag. Guo's group [125] reported that the low-temperature sputtered NiO_x nano-HTL to substitute that prepared via solution method resulted in remarkably high photocurrent and improved PCE to 11.6% (Figure 9). The sputtered NiO_x film is hard to get better PCE in conventional structure PSCs with polymers or small molecules HTLs [127], most likely due to the harm of sputtering ion on the PAL. However, solution processed NiO_x was shown not necessarily of poor quality. Yang's group [129] reported a PSCs based on all-metal-ox-

ide charge transport layers (that has p-type NiO_x and n-type ZnO nanoparticles as hole and electron transport layers, respectively) that show 16.1% efficiency and significantly improved stability compared with cells made with organic layers (Figure 10). The result is very encouraging as it shows both processing advantage and lifetime enhancement—two key

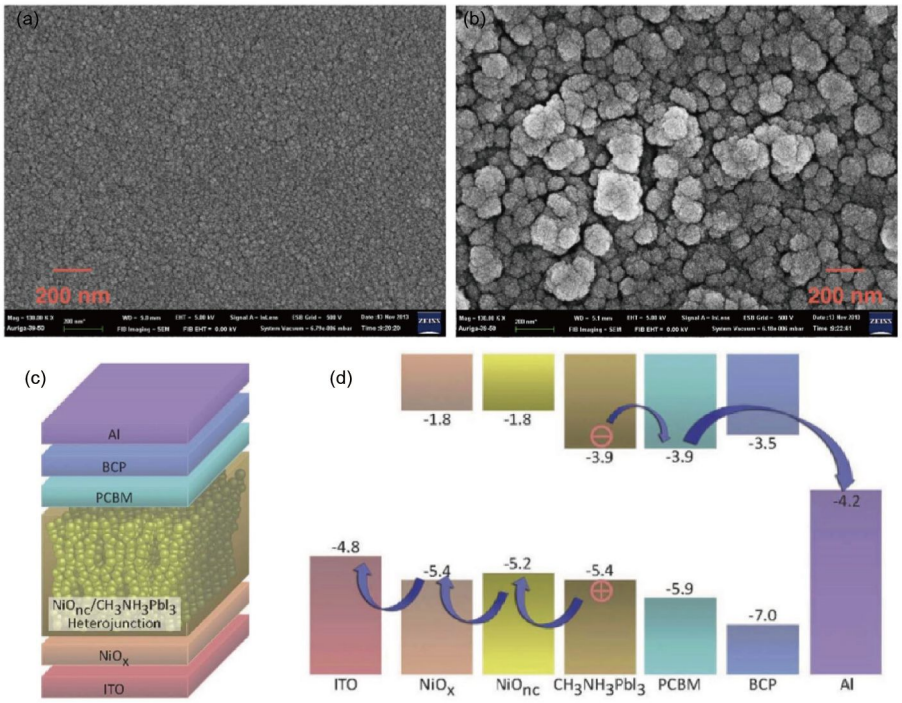

Figure 9 Scanning electron microscope (SEM) images of (a) NiO_x thin film and (b) NiO nanocrystal, (c) schematic and (d) the energy-level diagram of the device [124,125] (color online).

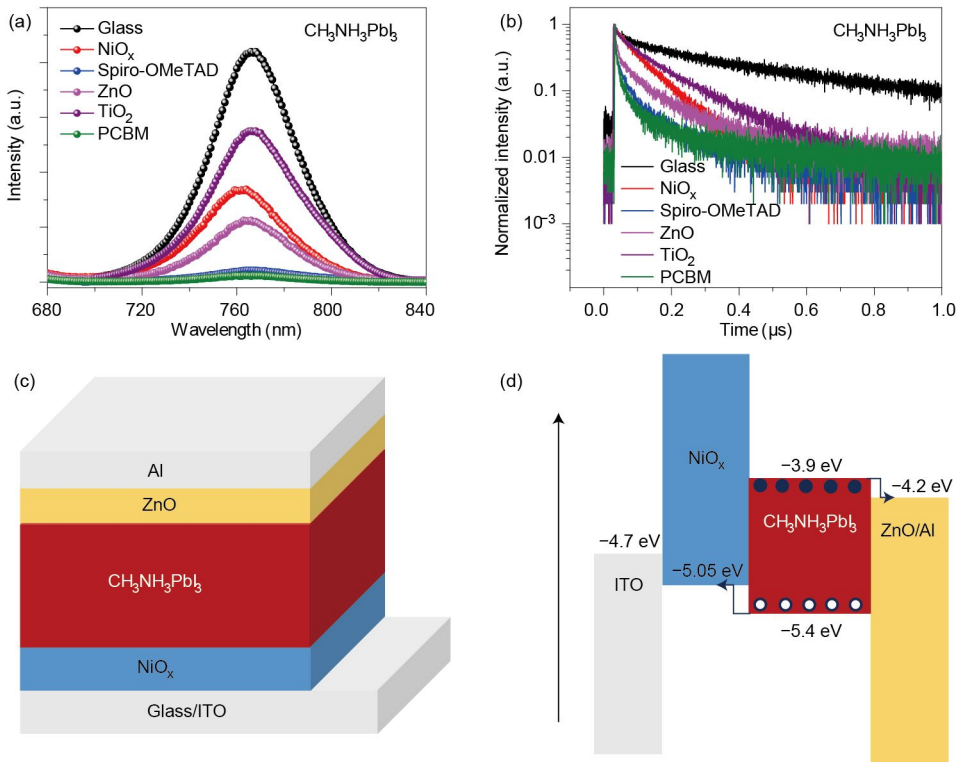

Figure 10 (a) Photoluminescence and (b) TRPL data of $CH_3NH_3PbI_3$ contacted with different interfaces; (c) overall device structure, consisting of glass; (d) energy band alignment of the metal-oxide-based perovskite solar cell [129] (color online).

issues in perovskite solar cell technology. Table 2 summarized the application of various TMOs as HTL in PSC, including NiO_x HTL.

Seok's group [130] used the PLD method to obtain a well-ordered nanostructured NiO_x film with high optical transparency. Based on this nanostructure, the corresponding PSC obtained a huge improved PCE of 17.3%. Likewise, Han's group [137] prepared ultrathin compact NiO_x film by a facile spray pyrolysis method. Between NiO film and $CH_3NH_3PbI_3$ layer, an added inert mesoporous Al_2O_3 scaffold was found useful to fill pinholes of the ultrathin NiO_x layer (Figure 11), and form an effective blocking roles of the hybrid interfacial layer, which leads to a high PCE exceeding 13%. However, the hole-transport paths could be constrained to the perovskite channels since the hole-injection from $CH_3NH_3PbI_3$ to Al_2O_3 is energetically forbidden.

With all the progress on NiO_x prepared from different methods, nickel oxide has the low hole-mobility and the defective adsorbate, including hydroxyl groups and oxyhydroxides, on its surface [68,69]. Therefore, the effective strategies, such as doping NiO_x with high conductive metal ions which generally possess unique electronic and structural effects as well as easy solution-processable way to be incorporated in, were explored [131,132].

Jen *et al.* [131] used copper as dopant to make the electrical conductivity of NiO_x film two orders magnitude higher compared to the non-doped NiO_x, which can improve the ability of hole-extracting from the perovskite PAL, and decrease the series resistance of the device. Consequently, the PSCs based on Cu doped NiO_x (Cu:NiO_x) HTL obtained an impressive PCE up to 15.4% comparing to that based on non-doped NiO_x HTL. Subsequently, they further explored the properties of Cu:NiO_x, and found that Cu:NiO_x film can obtain both homogeneous morphology and high crystallinity by a low temperature (~150 °C), solution processable method via combustion [132]. It is worth noting that this Cu:NiO_x film exhibited

Table 2 Performance parameters of PSCs with TMO films as interface layers

Structure of device [a)]	HTL prepared method and annealing temperature	The active or mask area of the device	V_{oc} (V)	J_{sc} (mA/cm^2)	FF (%)	PCE (%)	Ref.
ITO/NiO_x/$MAPbI_3$/PCBM/BCP/Al	Solution deposition, 300 °C	0.06 cm^2	0.92	12.43	68	7.8	[63]
ITO/NiO_x/$MAPbI_3$/PCBM/BCP/Ag	Solution deposition	0.10 cm^2	0.994	20.4	66.8	13.6	[126]
ITO/NiO_x/NiO_{nc}/$MAPbI_3$/PCBM/BCP/Al	sputtering deposition, 150 °C		0.96	19.8	61.0	11.6	[125]
ITO/NiO_x/$CH_3NH_3PbI_3$/ZnO/Al	Solution deposition, 300 °C	0.10 cm^2	1.01	21.0	76.0	16.1	[129]
ITO/NiO_x/$CH_3NH_3PbI_3$/PCBM/LiF/Al	Pulsed laser, 200 °C	0.09 cm^2	1.06	20.2	81.3	17.3	[130]
ITO/Cu:NiO_x/$MAPbI_3$/PCBM/C60/Ag	Sol-gel deposition, 275 °C	0.0314 cm^2	1.11	19.17	72.0	15.40	[131]
ITO/ NiO_x/$MAPbI_3$/PCBM/C60/Ag	Sol-gel deposition, 275 °C	0.0314 cm^2	1.08	14.42	58.0	8.94	[131]
ITO/Cu:NiO_x/$MAPbI_3$/C60/Bis-C60/Ag	Combustion method, 150 °C	0.0314 cm^2	1.05	22.23	76.0	17.74	[132]
ITO/Cu:NiO_x/$MAPbI_3$/C60/Bis-C60/Ag	Conventional sol-gel, 500 °C	0.0314 cm^2	1.05	20.53	72.0	15.52	[132]
ITO/UVO-Cu:Ni(ac)/$MAPbI_3$/PCBM/Al	Solution deposition, 245 °C		1.00	16.1	67.0	12.2	[133]
FTO/NiO_x(Li:Mg)/$MAPbI_3$/PCBM/Ti(Nb)O_x/Ag	Spray pyrolysis, 500 °C	>1 cm^2	1.09	20.4	83.0	18.4	[134]
ITO/Cu_2O_x/$MAPbI_3$/PCBM/Ca/A1	Chemical reaction method *in situ*, 100 °C	0.04 cm^2	1.07	16.52	75.51	13.35	[76]
ITO/CuO/$MAPbI_3$/PCBM//Ca/A1	Annealing, 250 °C	0.04 cm^2	1.06	15.82	72.54	12.16	[76]
ITO/CuO_x/$MAPbI_3$/PCBM/C60/BCP/Ag	Solution deposition, 80 °C	0.10 cm^2	1.01	20.1	70.6	14.4	[135]
ITO/CuO_x/$MAPbI_{3-x}Cl_x$/PCBM/C60/BCP/Ag	Solution deposition, 80 °C	0.10 cm^2	1.11	22.5	75.8	19.0	[135]
FTO/Cu:CrO_x/$MAPbI_3$/PCBM/Al	Sputtering deposition, 200 °C	0.09 cm^2	0.99	16.33	70.0	11.48	[37]
ITO/WO_3/$MAPbI_3$/PCBM/Al	Solvo-thermal method, 200 °C	0.04 cm^2	0.92	18.10	64.0	7.68	[136]

a) BCP: bathocuproine.

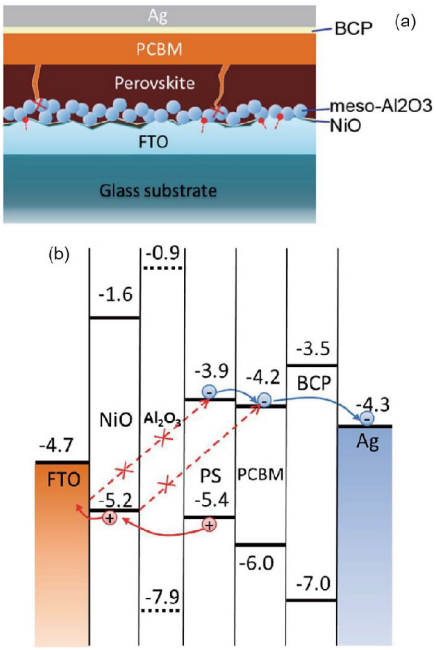

Figure 11 (a) Cell configuration and (b) the cell energy level (versus vacuum) diagram of the inverted PSC with the structure of FTO/NiO/meso-Al_2O_3/$CH_3NH_3PbI_3$/PCBM/BCP/Ag [137] (color online).

a better photoluminescence (PL) quenching efficiency with $CH_3NH_3PbI_3$ than that prepared via conventional sol-gel method, indicating more efficient hole-extraction/collection capability. As a result, the corresponding PSCs has afforded an impressive PCE of 17.8% from its original value of 15.52% [132]. The Cu:NiO_x-based solar cell shows markedly improved air stability as compared to the PEDOT:PSS-based device. The PCE of the Cu:NiO_x-based device remains above 90% of the initial value even after 240 h of storage in air. In contrast, the PEDOT:PSS-based device degraded to <50% of its initial PCE within 144 h of storage in air. As aforementioned, this lower stability might originate from the acidic and hygroscopic characteristics of PEDOT:PSS [131].

In 2015, Han *et al.* [134] reported dual p-doping Mg^{2+} and Li^+ for NiO_x (Figure 12). Substitutional doping by Li^+ is to increase the p-conductivity of NiO_x, while Mg^{2+} was alloyed in the Li^+-doped nickel oxide film to compensate for the undesirable positive valence band energy shift caused by the incorporation of Li^+ into the lattice. Combined with n^+-doping TiO_x to extract selectively photo-generated charge carriers in an inverted planar $MAPbI_3$-PCBM film architecture, this leads to dramatic increase of the electrical conductivity in 10–20 nm

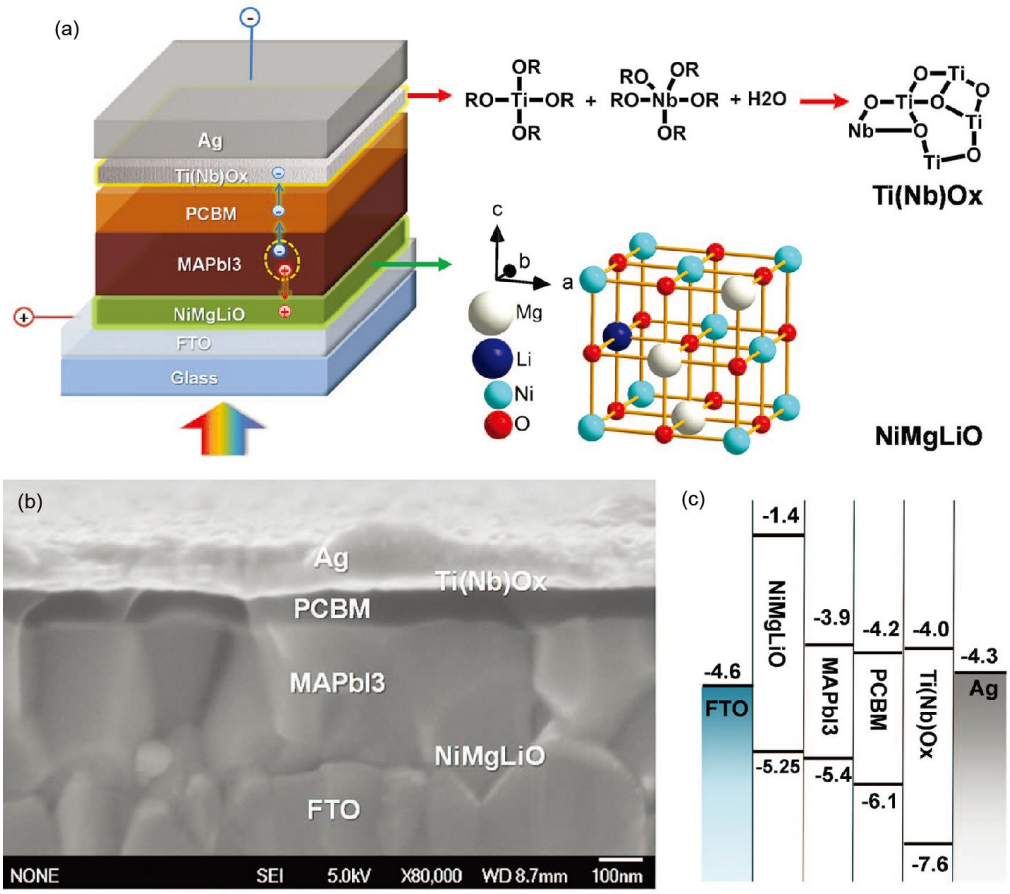

Figure 12 Structure and band alignments of the PSC. (a) Diagram of the cell configuration highlighting the doped charge carrier extraction layers. The right panels show the composition of Ti(Nb)O_x and the crystal structure of Li^+-doped $Ni_xMg_{1-x}O$, denoted as NiMg(Li)O. (b) A high-resolution crosssectional SEM image of a complete solar cell. (c) Band alignments of the solar cell [134] (color online).

thick oxide layer, reduces pinholes and local structural defects over large areas (>1 cm^2). Accordingly, the performance of PSC was improved by increasing the values of FF and V_{oc} to 0.827 and 1.083 V, respectively, leading to a PCE of 18.3%. Large size (>1 cm^2) PSCs with a PCE up to 16.2% was obtained. And the PSCs were stable with >90% of the initial PCE remaining after 1000 h of light soaking.

In addition, Jang's group [133] used UV-ozone irradiation to treat copper doped nickel acetate and increased its electrical conductivity by two orders magnitude (from 4.28×10^{-4} S/cm to 5.66×10^{-2} S/cm) (Figure 13), possibly due to a thin layer of Cu:NiO_x formed between copper doped nickel acetate and PAL. The charge extraction efficiency was enhanced, leading to better compatibility with the hole-transport layer and a 12.2% PCE. This unique low-temperature process deserves further attention with its compatibility with a variety of substrates and electrodes.

3.2 Copper oxides HTM

Copper oxides (CuO_x) is not viewed as the optimal window material because of the narrow band gaps of CuO (1.3–2.0 eV) and Cu_2O (2.1–2.3 eV) [71–73,76,77]. Therefore, it is not as much a focused HTL material for solar cell devices as NiO. On the other hand, as the typical HTL is optically thin—10–50 nm, the effect of HTL light absorption maybe ignorable, if its hole transport property and energy level etc. are superior.

Li's group [52] adopted an *in situ* oxidization method to oxidize copper acetylacetonate ($Cu(acac)_2$) film to CuO_x film, and use it as HTL in OSCs. They achieved a PCE exceeds to 7% in the structure of ITO/CuO_x/PBDTTT-C:$PC_{70}BM$/Ca/Al (Figure 14). The OSC with CuO_x film as HTL by sol-gel method shows a lower 5.90% PCE with PBDTTT-C:$PC_{70}BM$ as active layer [138]. Xie and co-workers [71] developed a ultrasonic irradiation-assisted chemical reaction method, which is reacting $CuCl_2$ solution with tetramethylammonium hydroxide to produce CuO nanoparticles for HTL. It was found that ca. 8 nm nanocrystal of CuO can form a uniform surface on substrate, which favors the formation of a high-quality interface between CuO HTL and PAL. The OSC with a structure of ITO/CuO_x/PCDTBT:$PC_{71}BM$/Ca/Al reached a high PCE of 6.44%.

In perovskite solar cell, Ding and co-workers [76] developed a novel and facile low-temperature chemical reaction method, which is reacting CuI film with NaOH to produce Cu_2O film *in situ*, then CuO film was made by heating Cu_2O film in air (Figure 15). It was found that Cu_2O and CuO small size crystal favors the formation of a high-quality $CH_3NH_3PbI_3$ layer on top. Cu_2O and CuO can effectively quench the PL of $CH_3NH_3PbI_3$, and the low-lying valence bands of Cu_2O and CuO match well with $CH_3NH_3PbI_3$, which minimize the energy loss when function as HTLs in PSCs [76]. The corresponding PSCs reached a high PCE of 13.35% and 12.16%, respectively. Similarly, Wu *et al.* [139]

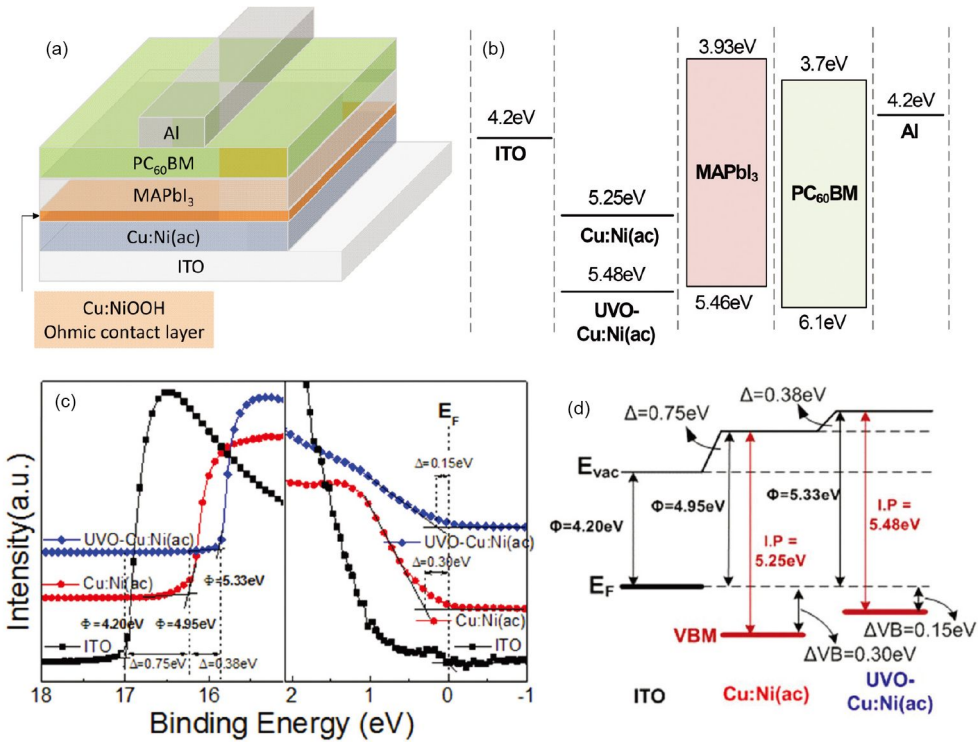

Figure 13 (a) Schematic device structure; (b) energy band diagram of the full solar device; (c) UPS spectra with the secondary-electron cutoff region and zoom-in of the valence band edge of Cu:Ni(ac) and UVO-Cu:Ni(ac) on the ITO substrate; (d) energy level alignment for the ITO/HTL junction [133] (color online).

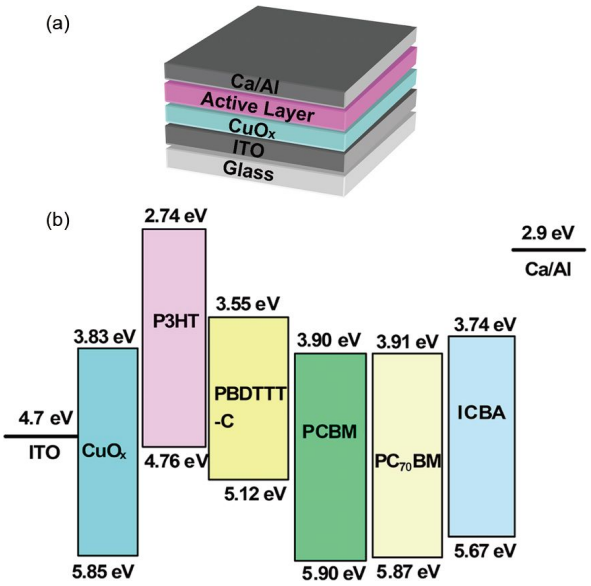

Figure 14 (a) Device structure of the polymer solar cells; (b) the HOMO and LUMO energy levels of the materials involved in the OSCs [52] (color online).

adopted a facile thermal oxidation method to preparing Cu_2O. Combining the merits of low cost, facile synthesis, and high device performance, ultrathin Cu_2O films fabricated via thermal oxidation hold promise for facilitating the developments of industrial-scale PSCs. Surprisingly, a simple UV-ozone treatment can *in situ* oxidize $Cu(acac)_2$ film into CuO_x. PCE up to 19% was achieved in the structure of ITO/CuO_x/$MAPbI_{3-x}Cl_x$/PCBM/C60/BCP/Al by Bian *et al*. [135], which introduced a novel Cl doping technique to improve the perovskite film morphology. The increased hole mobility, reduced intrinsic defects and charge carrier recombination in the film are claimed to responsible to a great enhancement of the device performance. Zhang *et al*. [140] introduced $CuGaO_2$ as a HTL for perovskite solar cell, both high efficiency of 18.51% and longer stability are achieved.

3.3 Chromium oxides HTL

Chromium oxides have various composition forms, such as Cr_2O, CrO, Cr_3O_4, Cr_2O_3, CrO_2, Cr_8O_{11}, and CrO_3. Among them, Cr_2O_3 has an excellent stability to resists aggressive oxidizing conditions, even aqua regia [32]. Amorphous and polycrystalline Cr_2O_3 materials have ca. 3.7 eV band-gap [141]. CrO_x film is a complex with Cr^{3+}, Cr^{4+} and Cr^{6+} oxidation states fabricated by radio frequency sputtering method at 200 °C, and exhibits p-type semiconducting behavior because chromium vacancies are the predominating defects [53,85–88]. When used as HTL of OSC, PCE up to 3.28% is achieved in the device structure of FTO/CrO_x (10 nm)/P3HT:PC60BM/Al. CrN in amorphous CrO_x film can prevent water dissociation and hydroxylation at defect sites on the CrO_x film surface to enhance the stability of CrO_x film, and reduce the electrical resistivity of films to improve the ability of collecting hole [88]. Li *et al*. [114] used $Cr(acac)_3$ film as the precursor, then treated it by UVO to obtain CrO_x film with Cr_2O_3, $Cr(acac)_3$, $CrO(OH)/Cr(OH)_3$ and CrO_3. This leads to a PCE of 6.55% in OSC structure of ITO/CrO_x/P3HT:ICBA/Ca/Al (Table 1). Although functioned as HTL, it was recently unambiguously demonstrated with direct and inverse photoemission spectroscopy measurements that Chromium oxides are n-type materials exhibiting very deep lying electronic states [37]. Thus, some group also used Chromium oxides as electron transfer layer [142,143].

However, the film with multivalence chromium cation may be harmful to perovskite material. When CrO_x was used as HTL in PSC, it is found that Cr^{6+} oxidation state would react with the degradation product of $CH_3NH_3PbI_3$ [32,37]. By Cu doping, Cr^{6+} oxidation state can be suppressed, possibly due to the formation of copper-chromium oxide in the Cu:CrO_x film. PCE up to 11.48% was achieved in the device structure of FTO/Cu:CrO_x/$MAPbI_3$/PCBM/Al. This study not only provides a novel HTL system for high performance and decently stable optoelectronic devices, but also reveals the

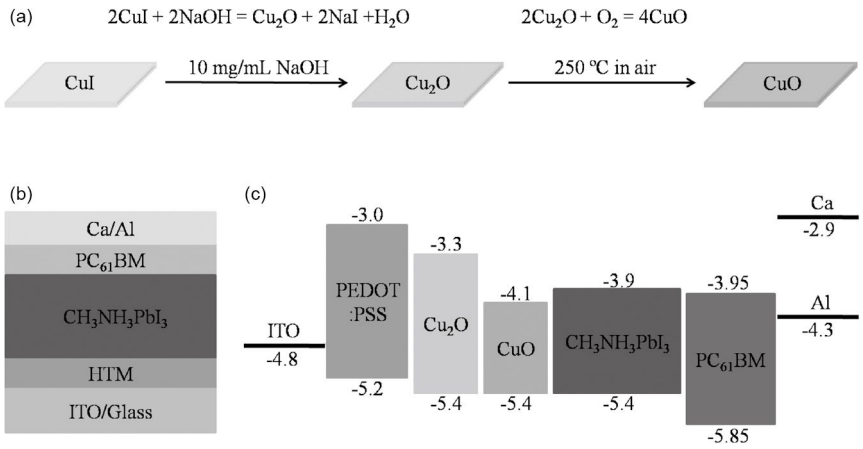

Figure 15 (a) Preparation process for Cu_2O and CuO films; (b) device structure; (c) energy level diagram [76].

importance of HTL doping for interface engineering.

3.4 Molybdenum oxide

Molybdenum oxide (MoO_x) film is a multivalent complex with Mo^{6+}, Mo^{5+} and Mo^{4+} oxidation states [78,79]. In 2006, Yang's group [56] firstly reported that transition metal oxides, MoO_3 and V_2O_5, can effectively substitute PEDOT:PSS as HTL in the OSCs. TMOs such as MoO_x soon gained large interest due to their mechanical and electrical robustness, low-cost, visible-light transparency, excellent environmental stability, good charge-transport properties, and the controllability of their film morphology on nano- to micrometer length scales. Among the metal oxides HTLs, MoO_3 is one of the most attractive TMOs owing to its relatively good hole-mobility, environmental stability, and transparency as HTL of OSC. Therefore, many research groups have tried to improve the hole-mobility and stability of inorganic oxide HTL. Various fabrication methods, such as thermal evaporation [56,95], sol-gel method [2,78,81], sputtering deposition [97], UV-ozone [98] and plasma [99] treatment have been employed to prepare MoO_3 HTLs.

Low-temperature-annealed sol-gel-derived MoO_x has the valence band edge at 5.4 eV, the conduction band edge at 2.3 eV [2], and a WF of 5.2 eV [83]. A PCE of 5.86% was observed from OSCs with a device structure of ITO/MoO_x/PBDTDTNT:$PC_{71}BM$/Al.

Heeger and co-workers [81] adapted solution method to prepare MoO_3 film, but found the Fermi level is pinned at 5.0 eV, an EA of 4.9 eV, and IE of 8.2 eV, i.e., it is an n-type material. This is further strengthened by the work of Lu and co-workers [79]. The sub-gap state (at 5.5 eV, Figure 7) resulted from Mo^{5+} species affected the device performance. When the density of such states was minimized, OSCs with performances comparable to PEDOT:PSS modified anodes could be achieved, and was up to 3.8% PCE in the structure of ITO/MoO_x/P3HT:$PC_{61}BM$/Al [81]. The OSCs with MoO_x as HTL can retain more than 75% of their initial short-circuit current density after 800 h. On the contrary, the reference device with the PEDOT:PSS layer exhibits fast degradation of its operational characteristics, resulting in a nearly zero current density after 120 h. MoO_x films by thermal evaporation were found to have WF at 5.4 eV. The films are composed of mainly Mo^{6+} (the small signal from Mo^{5+} is barely detectable), which implies that the chemical composition of the MoO_x films is close to the stoichiometric MoO_3 (Figure 16) [115]. Its energy level matches well with that of donor material PCDTBT, and the 6.50% PCE was obtained in the structure of ITO/MoO_x/PCDTBT:$PC_{70}BM$/TiO_x/Al. The structure with dual metal oxide layers as the carrier transport layers (HTL&ETL) provides protection of organic photoactive layer, which helps device stability.

The high EA enables the HOMO of many organic semiconductors to possess a sufficient density of states, which over-

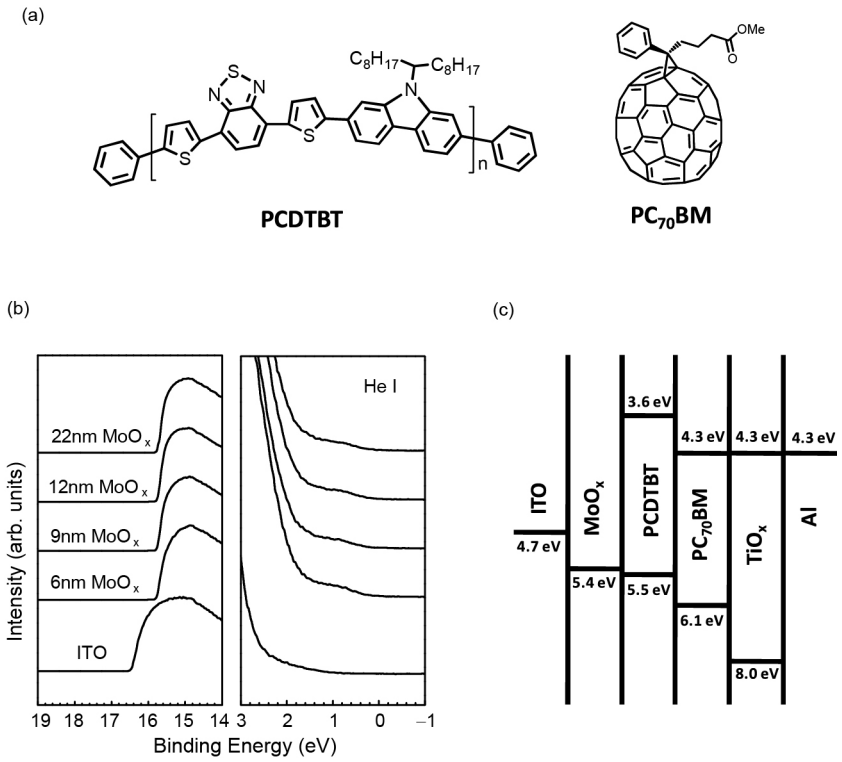

Figure 16 (a) Molecular structures of PCDTBT and $PC_{70}BM$; (b) UPS spectra of ITO and MoO_x films on ITO; (c) energy level diagram of the component materials in PCDTBT:$PC_{70}BM$ solar cells fabricated with MoO_x as HTL [115].

laps with the empty MoO_3 conduction band states to allow the ground state hole of organic semiconductor transferring to MoO_3 [91,144]. Moreover, the local electron depletion of the donor and acceptor at the interface would reduce back-contact recombination of the electrons from acceptors, while improving hole-collection from the donor materials at the interface. Such a situation may explain why n-type MoO_3 modified anodes have been so successfully used as a HTL in OSCs [81,115]. Because of its significantly deeper valence band edge, holes are transported to ITO through MoO_x gap states, not through the valence band of MoO_x [78]. This hole-selective behavior can be explained by invoking band bending at the MoO_x/organic interface which could partially block electrons [55]. Therefore, a p-type semiconductor is an essential but not necessary requirement for HTLs.

Although n-type MoO_x has been successfully used as HTL of OSCs, the hole-recombination occurs inevitably in the MoO_x/organic interface due to smaller band bending potential barrier at the interface. If p-type MoO_x can be obtained, carrier recombination at the interface can be effectively blocked. Fang's group [54] reported a sulfur-doped molybdenum oxide (S-MoO_3) film by sputtering method, and found that the partially occupied Mo 4d-bands of Mo^{5+} and Mo^{4+} states can be modulated by sulfur doping, which influences the valence electronic structure of S-MoO_3. These orbitals overlap interrelation push the valence band close to S-MoO_3's Fermi level, thus make it into a p-type semiconductor (Figure 17(a, b)). As a result, high efficiency approaching 3.7% based on S-MoO_x HTL has been achieved. Meanwhile, a double-layer MoO_3/MoS_2 film from MoS_2 by UVO *in-situ* growth was used as HTL in order to solve the recombination problem that occurs inevitably in the MoO_x/organic interface. It is because a smaller EA for MoS_2 film not only block effectively the electron from the exciton dissociation (Figure 17(c)), but also improve the ability of hole-transferring [55]. OSCs based on MoO_3/MoS_2 HTL showed an impressive PCE up to 4.15% (Figure 17) in P3HT:PCBM system.

Since MoO_x possesses a good charge-transport property, its ability of collecting-hole is far lower than the expectations. Some groups attempt to increase the electrical conductivity of MoO_x by inserting a thin metal, and make MoO_x HTL into sandwich structure without sacrificing their transmittance [100–102]. For example, Shao *et al*. [107] used a blend of MoO_3 and PEDOT:PSS as HTL in OSC. PCE increases from 5.5% to 6.4%, comparing to the reference pristine PEDOT:PSS-based device. More importantly, the device with MoO_3-PEDOT:PSS HTL shows considerably improved stability, with the PCE remaining at 80% of its original value when stored in ambient air in the dark for 10 d.

MoO_3 seem to be suitable for high stability HTL. However, it is not physically tough enough to the acidity of CH_3NH_3I with it as the HTL of inverted PSC, and can only be used on top of perovskite layer [145].

3.5 Tungsten oxide HTL

Tungsten oxide WO_3 possesses a higher WF of ~6.65 eV prepared by evaporation. Though contamination with ambient atmosphere can reduce its WF (e.g. ~5.7 eV), it nevertheless enables good charge carrier injection. Consequently, they have been used for hole-injection into wide band-gap emitters in small molecule organic light emitting diodes that were fabricated by thermal evaporation [80]. In 2009, Dong's group [146] explored the use of WO_3 by thermal evaporation in inverted PSCs, and found that WO_3 efficiently extracts holes and suppresses electrons from the active layer due to the high WF. Brabec and co-workers [116] demonstrated solution-processed WO_3 as HTL in OSCs with active layers comprising either P3HT or Si-PCPDTBT mixed with a fullerene derivative. The low-temperature (80 °C) annealed and alcohol-based WO_3 nanoparticle dispersion fullfill all requirements for the application on plastic substrates and on top of organic active layers. OSCs based on the structure of ITO/WO_3/Si-PCPDTBT:$PC_{70}BM$/Ca/Ag showed an impressive PCE up to 4.8%. Although WO_3 is n-type semiconductor, W^{5+} in the WO_3 film maybe act as the gap state, and holes are transported

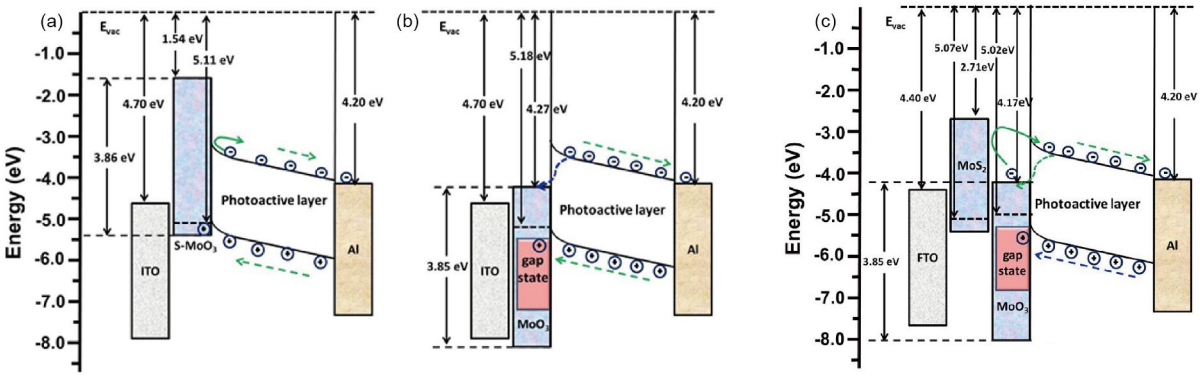

Figure 17 Schematic energy level diagrams of devices components referenced to the vacuum level. (a) S-MoO_3; (b) MoO_3; (c) MoO_3/MoS_2 [54,55] (color online).

to anode via gap-state, not the valence band of WO_3. Recently, plasma treated tungsten (VI) isopropoxide was used to obtain WO_3 HTL. The PCEs of the corresponding OSCs based on P3HT:$PC_{61}BM$ (wide bandgap polymer) and PBDTTT-C:$PC_{71}BM$ (narrow bandgap polymer) were improved by 24% (from 3.84% to 4.76%) and 27% (from 5.91% to 7.50%), respectively. The device for WO_3 HTL retains above 80% of its initial value after 500 h, which is more stability that that for PEDOT:PSS-device [147].

In order to achieve a large reduction in the cost of the transparent electrode, Hatton *et al*. [148] reported a combination of ultra-thin bilayer of Cu and tungsten sub-oxide (WO_{3-x}) which derives its exceptional optical and electrical properties from spontaneous solid-state diffusion of Cu into the adjacent WO_{3-x} layer at room temperature. The un-patterned Cu electrode can perform at least as well as ITO glass in ca. 6% efficient inverted OSCs by trapping light in a resonant optical cavity.

Li [136] reported a simple solvo-thermal method to fabricate WO_3 nanocrystals as the HTL in an inverted PSC. The diffraction peaks of WO_3 nanocrystals can be readily indexed to the orthorhombic phase WO_3, which could be an important factor for a 7.68% PCE achievement with it as the HTL of PSC.

3.6 Vanadium oxide HTL

V_2O_5 is also a good HTL candidate in solar cells [56]. Chuang *et al*. [117] showed V_2O_5 has a narrow band-gap of 2.42 eV, a low EA of 2.94 eV and deep IE about 5.36 eV, which indicates that it can form an efficient hole collection junction with the OSC [112]. However, Riedl *et al*. [82] determined V_2O_5 to be highly n-type, in contrast to the assumed p-type behavior, with a large WF and a very low lying valence band. The layers contain gap states due to oxygen deficiencies close to the Fermi level of the material. To date, solution processed V_2O_5 HTLs have been synthesized by multistep techniques, for example, spin-coating a suspension of V_2O_5 nano-particulates obtained from the hydrolysis of vanadium (III) acetyl acetate [149], or a suspension of V_2O_5 obtained after the reaction between the metal powder and H_2O_2 [150]. The most widespread fabrication method is the application of thermal evaporation, sol-gel make from vanadium (V) oxytriisopropoxide [82,112]. As early as in 2006, Yang's group [56,57] reported that thermally evaporated V_2O_5 can effectively substitute PEDOT:PSS as HTL in the OSCs. Chuang *et al.* [117] adopted VO_x as HTL in ITO/ZnO/a-PTPTBT:PCBM/VO_x/Ag structure. The constructed devices show enhanced performance with the studied polymers through increasing the J_{sc} value and the devices are highly durable, which shows the benefit of vanadium oxides sol-gel technique for OSC long-term stability.

In 2013, Snaith *et al*. [123] firstly attempted to adopted V_2O_5 as HTL in FTO/V_2O_5/$CH_3NH_3PbI_{3-x}Cl_x$/PCBM/TiO_x/Al, but attained poor photovoltaic performance. Soon after, Lu's group [151] enhanced the PCE of the device ITO/V_2O_5/$CH_3NH_3PbI_{3-x}Cl_x$/PCBM/Rhodamine/LiF/Ag up to 5.1%. Furthermore, they developed firstly a method resembling a cocoon-to silk fiber reeling process to fabricate layered V_2O_5/PEDOT nano-belts consisting of V_2O_5 atomic bilayers intercalated with PEDOT. With a 40 nm uniform and compact V_2O_5/PEDOT nano-belts on ITO substrate as HTL, the PSCs reached a PCE of 8.4%. Cell efficiency tests over 7 d revealed that PSCs fabricated with V_2O_5/PEDOT nano-belts as HTL retained the initial PCE, which is very encouraging.

4 Conclusions

In summary, as key components in organic polymer and perovskite solar cells, HTL materials play an important role in determining the performance of solar cells. Transition metal oxide semiconductors, including NiO, MoO_3, V_2O_5, WO_3, CuO_x and CrO_x, using as HTLs in OSC and PSCs are reviewed in the article.

These TMOs offer rich HTL alternatives in the exciting field of OSCs and PSCs. Enormous research efforts to improve the hole-mobility and stability of inorganic oxide HTL, various fabrication method and device engineering have been employed to achieve the desired optoelectronic properties, tunable energy levels and WFs, improved interfacial compatibility, good chemical/physical stability, etc.

Looking forward, besides dominate efforts on TMO along, doping TMOs is a potentially significant direction to adjust work function, achieve high carrier mobility, even transmittance and stability. These unique merits can lead to high performance OSCs and PSCs with extraordinary stability. For example, cesium doping of TiO_2 [152], MoO_x and VO_x [153] were successfully conducted to modify ETL and HTL in OSCs. These metal oxide semiconductors are complex with the multivalence state of metal cation, which is linked to defects in the TMOs. On the one side, the defects may: (1) improve the interfacial contact between the anode and photoactive layer; (2) intensify the ability of hole-collecting; (3) adjust the energy levels with doping to better match that of the anode (or photoactive). The other side is that the adsorption effect of surface defects can delay carrier migration, and results in additional recombination, which affect the PCE and stability of the devices.

Further investigation of solution processable TMO HTL is generally favorable. How to reduce the TMO conversion temperature from solution state to facilitate high performance flexible device is critically important for the future commercialization of the technologies. Technically, how to effectively adjust the valence states of metal cation in HTL film under low-temperature is usually a huge challenge for improving the PCE and stability of the devices.

The TMOs will continuously to be an active research area in OSC and PSC, due to their contribution in efficiency, stability and even manufacturability.

Acknowledgments This work was supported by the Project of Strategic Importance provided by The Hong Kong Polytechnic University (1-ZE29), the Natural Science Foundation of Hubei Province (2014CFB275), the Special (2016T90724, 2014T70735) and General (2015M572187, 2013M531737) Postdoctoral Science Foundation of China, the National High Technology Research and Development Program (2015AA050601), and the National Natural Science Foundation of China (61376013, 91433203, 11674252).

Conflict of interest The authors declare that they have no conflict of interest.

1 Günes S, Neugebauer H, Sariciftci NS. *Chem Rev*, 2007, 107: 1324–1338
2 Yang T, Wang M, Cao Y, Huang F, Huang L, Peng J, Gong X, Cheng SZD, Cao Y. *Adv Energy Mater*, 2012, 2: 523–527
3 Li G, Zhu R, Yang Y. *Nat Photon*, 2012, 6: 153–161
4 Zhang S, Ye L, Zhao W, Yang B, Wang Q, Hou J. *Sci China Chem*, 2015, 58: 248–256
5 Dou L, You J, Hong Z, Xu Z, Li G, Street RA, Yang Y. *Adv Mater*, 2013, 25: 6642–6671
6 Zhao J, Li Y, Yang G, Jiang K, Lin H, Ade H, Ma W, Yan H. *Nat Energy*, 2016, 1: 15027
7 Kim J, Hong Z, Li G, Song TB, Chey J, Lee YS, You J, Chen CC, Sadana DK, Yang Y. *Nat Commun*, 2015, 6: 6391
8 Chen CC, Chang WH, Yoshimura K, Ohya K, You J, Gao J, Hong Z, Yang Y. *Adv Mater*, 2014, 26: 5670–5677
9 Liu Y, Zhao J, Li Z, Mu C, Ma W, Hu H, Jiang K, Lin H, Ade H, Yan H. *Nat Commun*, 2014, 5: 5293
10 Xie F, Choy WCH, Wang C, Li X, Zhang S, Hou J. *Adv Mater*, 2013, 25: 2051–2055
11 http://www.nrel.gov/pv/assets/images/efficiency_chart.jpg. Accessed on 2017-01-20
12 Kojima A, Teshima K, Shirai Y, Miyasaka T. *J Am Chem Soc*, 2009, 131: 6050–6051
13 Zhou H, Chen Q, Li G, Luo S, Song T, Duan HS, Hong Z, You J, Liu Y, Yang Y. *Science*, 2014, 345: 542–546
14 Yang WS, Noh JH, Jeon NJ, Kim YC, Ryu S, Seo J, Seok SI. *Science*, 2015, 348: 1234–1237
15 Xing G, Mathews N, Sun S, Lim SS, Lam YM, Grätzel M, Mhaisalkar S, Sum TC. *Science*, 2013, 342: 344–347
16 Stranks SD, Eperon GE, Grancini G, Menelaou C, Alcocer MJP, Leijtens T, Herz LM, Petrozza A, Snaith HJ. *Science*, 2013, 342: 341–344
17 Bi D, Tress W, Dar MI, Gao P, Luo J, Renevier C, Schenk K, Abate A, Giordano F, Correa Baena JP, Decoppet JD, Zakeeruddin SM, Nazeeruddin MK, Gra tzel M, Hagfeldt A. *Sci Adv*, 2016, 2: e1501170
18 Na SI, Wang G, Kim SS, Kim TW, Oh SH, Yu BK, Lee T, Kim DY. *J Mater Chem*, 2009, 19: 9045
19 Moulé AJ, Meerholz K. *Adv Funct Mater*, 2009, 19: 3028–3036
20 Campoy-Quiles M, Ferenczi T, Agostinelli T, Etchegoin PG, Kim Y, Anthopoulos TD, Stavrinou PN, Bradley DDC, Nelson J. *Nat Mater*, 2008, 7: 158–164
21 Salim T, Sun S, Abe Y, Krishna A, Grimsdale AC, Lam YM. *J Mater Chem A*, 2015, 3: 8943–8969
22 Sepalage GA, Meyer S, Pascoe A, Scully AD, Huang F, Bach U, Cheng YB, Spiccia L. *Adv Funct Mater*, 2015, 25: 5650–5661
23 Zhang J, Zhang M, Sun RQ, Wang X. *Angew Chem*, 2012, 124: 10292–10296
24 Yao C, Xu X, Wang J, Shi L, Li L. *ACS Appl Mater Interfaces*, 2013, 5: 1100–1107
25 Ma H, Yip HL, Huang F, Jen AKY. *Adv Funct Mater*, 2010, 20: 1371–1388
26 Steim R, Kogler FR, Brabec CJ. *J Mater Chem*, 2010, 20: 2499–2512
27 Jørgensen M, Norrman K, Krebs FC. *Sol Energy Mater Sol Cells*, 2008, 92: 686–714
28 Norrman K, Gevorgyan SA, Krebs FC. *ACS Appl Mater Interfaces*, 2009, 1: 102–112
29 Norrman K, Madsen MV, Gevorgyan SA, Krebs FC. *J Am Chem Soc*, 2010, 132: 16883–16892
30 Schäfer S, Petersen A, Wagner TA, Kniprath R, Lingenfelser D, Zen A, Kirchartz T, Zimmermann B, Würfel U, Feng X, Mayer T. *Phys Rev B*, 2011, 83: 165311
31 You J, Yang YM, Hong Z, Song TB, Meng L, Liu Y, Jiang C, Zhou H, Chang WH, Li G, Yang Y. *Appl Phys Lett*, 2014, 105: 183902
32 Kaltenbrunner M, Adam G, Głowacki ED, Drack M, Schwödiauer R, Leonat L, Apaydin DH, Groiss H, Scharber MC, White MS, Sariciftci NS, Bauer S. *Nat Mater*, 2015, 14: 1032–1039
33 Xiao J, Shi J, Li D, Meng Q. *Sci China Chem*, 2015, 58: 221–238
34 Wei J, Zhao Y, Li H, Li G, Pan J, Xu D, Zhao Q, Yu D. *J Phys Chem Lett*, 2014, 5: 3937–3945
35 O'Regan BC, Barnes PRF, Li X, Law C, Palomares E, Marin-Beloqui JM. *J Am Chem Soc*, 2015, 137: 5087–5099
36 Christians JA, Miranda Herrera PA, Kamat PV. *J Am Chem Soc*, 2015, 137: 1530–1538
37 Qin PL, Lei HW, Zheng XL, Liu Q, Tao H, Yang G, Ke WJ, Xiong LB, Qin MC, Zhao XZ, Fang GJ. *Adv Mater Interfaces*, 2016, 3: 1500799
38 Park JH, Park JI, Kim DH, Kim JH, Kim JS, Lee JH, Sim M, Lee SY, Cho K. *J Mater Chem*, 2010, 20: 5860–5865
39 Jung JW, Jo WH. *Adv Funct Mater*, 2010, 20: 2355–2363
40 Park JH, Kim JS, Lee JH, Lee WH, Cho K. *J Phys Chem C*, 2009, 113: 17579–17584
41 Chen LM, Xu Z, Hong Z, Yang Y. *J Mater Chem*, 2010, 20: 2575–2598
42 Xu Y, Shi J, Lv S, Zhu L, Dong J, Wu H, Xiao Y, Luo Y, Wang S, Li D, Li X, Meng Q. *ACS Appl Mater Interfaces*, 2014, 6: 5651–5656
43 Qin P, Tetreault N, Dar MI, Gao P, McCall KL, Rutter SR, Ogier SD, Forrest ND, Bissett JS, Simms MJ, Page AJ, Fisher R, Grätzel M, Nazeeruddin MK. *Adv Energy Mater*, 2015, 5: 1400980
44 Heo JH, Im SH, Noh JH, Mandal TN, Lim CS, Chang JA, Lee YH, Kim H, Sarkar A, Nazeeruddin MK, Grätzel M, Seok SI. *Nat Photon*, 2013, 7: 486–491
45 Yang G, Tao H, Qin P, Ke W, Fang G. *J Mater Chem A*, 2016, 4: 3970–3990
46 Kim HS, Lee CR, Im JH, Lee KB, Moehl T, Marchioro A, Moon SJ, Humphry-Baker R, Yum JH, Moser JE, Grätzel M, Park NG. *Sci Rep*, 2012, 2: 591–598
47 Lee MM, Teuscher J, Miyasaka T, Murakami TN, Snaith HJ. *Science*, 2012, 338: 643–647
48 Xu B, Sheibani E, Liu P, Zhang J, Tian H, Vlachopoulos N, Boschloo G, Kloo L, Hagfeldt A, Sun L. *Adv Mater*, 2014, 26: 6629–6634
49 Zhu Z, Bai Y, Zhang T, Liu Z, Long X, Wei Z, Wang Z, Zhang L, Wang J, Yan F, Yang S. *Angew Chem Int Ed*, 2014: 12571–12575
50 Leguy AMA, Hu Y, Campoy-Quiles M, Alonso MI, Weber OJ,

Azarhoosh P, van Schilfgaarde M, Weller MT, Bein T, Nelson J, Docampo P, Barnes PRF. *Chem Mater*, 2015, 27: 3397–3407
51 Irwin MD, Buchholz DB, Hains AW, Chang RPH, Marks TJ. *Proc Natl Acad Sci USA*, 2008, 105: 2783–2787
52 Xu Q, Wang F, Tan Z, Li L, Li S, Hou X, Sun G, Tu X, Hou J, Li Y. *ACS Appl Mater Interfaces*, 2013, 5: 10658–10664
53 Qin P, Fang G, Sun N, Fan X, Zheng Q, Chen F, Wan J, Zhao X. *Thin Solid Films*, 2011, 519: 4334–4341
54 Qin P, Fang G, Cheng F, Ke W, Lei H, Wang H, Zhao X. *ACS Appl Mater Interfaces*, 2014, 6: 2963–2973
55 Qin P, Fang G, Ke W, Cheng F, Zheng Q, Wan J, Lei H, Zhao X. *J Mater Chem A*, 2014, 2: 2742–2756
56 Shrotriya V, Li G, Yao Y, Chu CW, Yang Y. *Appl Phys Lett*, 2006, 88: 073508
57 Li G, Chu CW, Shrotriya V, Huang J, Yang Y. *Appl Phys Lett*, 2006, 88: 253503
58 Meyer J, Hamwi S, Kröger M, Kowalsky W, Riedl T, Kahn A. *Adv Mater*, 2012, 24: 5408–5427
59 Manders JR, Tsang SW, Hartel MJ, Lai TH, Chen S, Amb CM, Reynolds JR, So F. *Adv Funct Mater*, 2013, 23: 2993–3001
60 Ohta H, Kamiya M, Kamiya T, Hirano M, Hosono H. *Thin Solid Films*, 2003, 445: 317–321
61 Fujimori A, Minami F. *Phys Rev B*, 1984, 30: 957–971
62 Ai L, Fang G, Yuan L, Liu N, Wang M, Li C, Zhang Q, Li J, Zhao X. *Appl Surface Sci*, 2008, 254: 2401–2405
63 Jeng JY, Chen KC, Chiang TY, Lin PY, Tsai TD, Chang YC, Guo TF, Chen P, Wen TC, Hsu YJ. *Adv Mater*, 2014, 26: 4107–4113
64 St Uhlenbrock, Scharfschwerdt C, Neumann M, Illing G, Freund HJ. *J Phys Condens Mat*, 1992, 4: 7973
65 Kim KS, Winograd N. *Surf Sci*, 1974, 43: 625–643
66 Sasi B, Gopchandran KG. *Nanotechnology*, 2007, 18: 115613
67 Jiang F, Choy WCH, Li X, Zhang D, Cheng J. *Adv Mater*, 2015, 27: 2930–2937
68 Ratcliff EL, Meyer J, Steirer KX, Garcia A, Berry JJ, Ginley DS, Olson DC, Kahn A, Armstrong NR. *Chem Mater*, 2011, 23: 4988–5000
69 Han SY, Lee DH, Chang YJ, Ryu SO, Lee TJ, Chang CH. *J Electrochem Soc*, 2006, 153: 382–385
70 Steirer KX, Ndione PF, Widjonarko NE, Lloyd MT, Meyer J, Ratcliff EL, Kahn A, Armstrong NR, Curtis CJ, Ginley DS, Berry JJ, Olson DC. *Adv Energy Mater*, 2011, 1: 813–820
71 Zhang J, Wang J, Fu Y, Zhang B, Xie Z. *RSC Adv*, 2015, 5: 28786–28793
72 Al-Jawhari HA, Caraveo-Frescas JA, Hedhili MN, Alshareef HN. *ACS Appl Mater Interfaces*, 2013, 5: 9615–9619
73 Fortunato E, Figueiredo V, Barquinha P, Elamurugu E, Barros R, Gonçalves G, Park SHK, Hwang CS, Martins R. *Appl Phys Lett*, 2010, 96: 192102
74 Wagner CD, Riggs WM, Davis LE, Moulder JE. *Handbook of X-Ray Photoelectron Spectroscopy*. Eden Prairie, Minnesota: Perkin-Elmer Corporation, 1979
75 Lee SW, Lee YS, Heo J, Siah SC, Chua D, Brandt RE, Kim SB, Mailoa JP, Buonassisi T, Gordon RG. *Adv Energy Mater*, 2014, 4: 1301916
76 Zuo C, Ding L. *Small*, 2015, 11: 5528–5532
77 Murali DS, Kumar S, Choudhary RJ, Wadikar AD, Jain MK, Subrahmanyam A. *AIP Adv*, 2015, 5: 047143
78 Wong KH, Ananthanarayanan K, Luther J, Balaya P. *J Phys Chem C*, 2012, 116: 16346–16351
79 Greiner MT, Chai L, Helander MG, Tang WM, Lu ZH. *Adv Funct Mater*, 2013, 23: 215–226
80 Höfle S, Bruns M, Strässle S, Feldmann C, Lemmer U, Colsmann A. *Adv Mater*, 2013, 25: 4113–4116
81 Jasieniak JJ, Seifter J, Jo J, Mates T, Heeger AJ. *Adv Funct Mater*, 2012, 22: 2594–2605
82 Zilberberg K, Trost S, Meyer J, Kahn A, Behrendt A, Lützenkirchen-Hecht D, Frahm R, Riedl T. *Adv Funct Mater*, 2011, 21: 4776–4783
83 Hammond SR, Meyer J, Widjonarko NE, Ndione PF, Sigdel AK, Garcia A, Miedaner A, Lloyd MT, Kahn A, Ginley DS, Berry JJ, Olson DC. *J Mater Chem*, 2012, 22: 3249–3254
84 Tokmoldin N, Griffiths N, Bradley DDC, Haque SA. *Adv Mater*, 2009, 21: 3475–3478
85 Ingle NJC, Hammond RH, Beasley MR. *J Appl Phys*, 2001, 89: 4631–4635
86 Qin P, Fang G, Sun N, Fan X, Zheng Q, Chen F, Wan J, Zhao X. *Appl Surface Sci*, 2011, 257: 3952–3958
87 Qin P, Fang G, Zeng W, Fan X, Zheng Q, Cheng F, Wan J, Zhao X. *Sol Energy Mater Sol Cells*, 2011, 95: 3311–3317
88 Qin P, Fang G, He Q, Sun N, Fan X, Zheng Q, Chen F, Wan J, Zhao X. *Sol Energy Mater Sol Cells*, 2011, 95: 1005–1010
89 Yi Y, Jeon PE, Lee H, Han K, Kim HS, Jeong K, Cho SW. *J Chem Phys*, 2009, 130: 094704
90 Chu CW, Li SH, Chen CW, Shrotriya V, Yang Y. *Appl Phys Lett*, 2005, 87: 193508
91 Kröger M, Hamwi S, Meyer J, Riedl T, Kowalsky W, Kahn A. *Org Electron*, 2009, 10: 932–938
92 Park JS, Lee BR, Lee JM, Kim JS, Kim SO, Song MH. *Appl Phys Lett*, 2010, 96: 243306
93 Meyer J, Zilberberg K, Riedl T, Kahn A. *J Appl Phys*, 2011, 110: 033710
94 Kyaw AKK, Sun XW, Jiang CY, Lo GQ, Zhao DW, Kwong DL. *Appl Phys Lett*, 2008, 93: 221107
95 Liu J, Shao S, Fang G, Meng B, Xie Z, Wang L. *Adv Mater*, 2012, 24: 2774–2779
96 Vasilopoulou M, Douvas AM, Georgiadou DG, Palilis LC, Kennou S, Sygellou L, Soultati A, Kostis I, Papadimitropoulos G, Davazoglou D, Argitis P. *J Am Chem Soc*, 2012, 134: 16178–16187
97 Cheng F, Fang G, Fan X, Huang H, Zheng Q, Qin P, Lei H, Li Y. *Sol Energy Mater Sol Cells*, 2013, 110: 63–68
98 Kato S, Ishikawa R, Kubo Y, Shirai H, Ueno K. *Jpn J Appl Phys*, 2011, 50: 071604
99 Frey GL, Reynolds KJ, Friend RH, Cohen H, Feldman Y. *J Am Chem Soc*, 2003, 125: 5998–6007
100 Jin H, Tao C, Velusamy M, Aljada M, Zhang Y, Hambsch M, Burn PL, Meredith P. *Adv Mater*, 2012, 24: 2572–2577
101 Tao C, Xie G, Liu C, Zhang X, Dong W, Meng F, Kong X, Shen L, Ruan S, Chen W. *Appl Phys Lett*, 2009, 95: 053303
102 Cattin L, Morsli M, Dahou F, Abe SY, Khelil A, Bernède JC. *Thin Solid Films*, 2010, 518: 4560–4563
103 Qiao L, Wang D, Zuo L, Ye Y, Qian J, Chen H, He S. *Appl Energy*, 2011, 88: 848–852
104 Wu JL, Chen FC, Hsiao YS, Chien FC, Chen P, Kuo CH, Huang MH, Hsu CS. *ACS Nano*, 2011, 5: 959–967
105 Kalfagiannis N, Karagiannidis PG, Pitsalidis C, Panagiotopoulos NT, Gravalidis C, Kassavetis S, Patsalas P, Logothetidis S. *Sol Energy Mater Sol Cells*, 2012, 104: 165–174
106 Reineck P, Lee GP, Brick D, Karg M, Mulvaney P, Bach U. *Adv Mater*, 2012, 24: 4750–4755
107 Shao S, Liu J, Bergqvist J, Shi S, Veit C, Würfel U, Xie Z, Zhang F. *Adv Energy Mater*, 2013, 3: 349–355

108 Yoon WJ, Berger PR. *Appl Phys Lett*, 2008, 92: 013306
109 Sgobba V, Guldi DM. *J Mater Chem*, 2008, 18: 153–157
110 Meyer J, Kröger M, Hamwi S, Gnam F, Riedl T, Kowalsky W, Kahn A. *Appl Phys Lett*, 2010, 96: 193302
111 DeLongchamp DM, Kline RJ, Fischer DA, Richter LJ, Toney MF. *Adv Mater*, 2011, 23: 319–337
112 Yan W, Ye S, Li Y, Sun W, Rao H, Liu Z, Bian Z, Huang C. *Adv Energy Mater*, 2016, 6: 1600474
113 Bai S, Cao M, Jin Y, Dai X, Liang X, Ye Z, Li M, Cheng J, Xiao X, Wu Z, Xia Z, Sun B, Wang E, Mo Y, Gao F, Zhang F. *Adv Energy Mater*, 2014, 4: 1301460
114 Tu X, Wang F, Li C, Tan Z, Li Y. *J Phys Chem C*, 2014, 118: 9309–9317
115 Sun Y, Takacs CJ, Cowan SR, Seo JH, Gong X, Roy A, Heeger AJ. *Adv Mater*, 2011, 23: 2226–2230
116 Stubhan T, Li N, Luechinger NA, Halim SC, Matt GJ, Brabec CJ. *Adv Energy Mater*, 2012, 2: 1433–1438
117 Chen CP, Chen YD, Chuang SC. *Adv Mater*, 2011, 3859–3863
118 Wong KH, Ananthanarayanan K, Heinemann MD, Luther J, Balaya P. *Sol Energy*, 2012, 86: 3190–3195
119 Sun N, Fang G, Qin P, Zheng Q, Wang M, Fan X, Cheng F, Wan J, Zhao X, Liu J, Carroll DL, Ye J. *J Phys D-Appl Phys*, 2010, 43: 445101
120 Sun N, Fang G, Qin P, Zheng Q, Wang M, Fan X, Cheng F, Wan J, Zhao X. *Sol Energy Mater Sol Cells*, 2010, 94: 2328–2331
121 Widjonarko NE, Schulz P, Parilla PA, Perkins CL, Ndione PF, Sigdel AK, Olson DC, Ginley DS, Kahn A, Toney MF, Berry JJ. *Adv Energy Mater*, 2014, 4: 1301879
122 Chen TL, Betancur R, Ghosh DS, Martorell J, Pruneri V. *Appl Phys Lett*, 2012, 100: 013310
123 Docampo P, Ball JM, Darwich M, Eperon GE, Snaith HJ. *Nat Commun*, 2013, 4: 2761–2766
124 Wang KC, Jeng JY, Shen PS, Chang YC, Diau EWG, Tsai CH, Chao TY, Hsu HC, Lin PY, Chen P, Guo TF, Wen TC. *Sci Rep*, 2014, 4: 4756
125 Wang KC, Shen PS, Li MH, Chen S, Lin MW, Chen P, Guo TF. *ACS Appl Mater Interfaces*, 2014, 6: 11851–11858
126 Li Y, Ye S, Sun W, Yan W, Li Y, Bian Z, Liu Z, Wang S, Huang C. *J Mater Chem A*, 2015, 3: 18389–18394
127 Cui J, Meng F, Zhang H, Cao K, Yuan H, Cheng Y, Huang F, Wang M. *ACS Appl Mater Interfaces*, 2014, 6: 22862–22870
128 Trifiletti V, Roiati V, Colella S, Giannuzzi R, De Marco L, Rizzo A, Manca M, Listorti A, Gigli G. *ACS Appl Mater Interfaces*, 2015, 7: 4283–4289
129 You J, Meng L, Song TB, Guo TF, Yang YM, Chang WH, Hong Z, Chen H, Zhou H, Chen Q, Liu Y, De Marco N, Yang Y. *Nat Nanotech*, 2015, 11: 75–81
130 Park JH, Seo J, Park S, Shin SS, Kim YC, Jeon NJ, Shin HW, Ahn TK, Noh JH, Yoon SC, Hwang CS, Seok SI. *Adv Mater*, 2015, 27: 4013–4019
131 Kim JH, Liang PW, Williams ST, Cho N, Chueh CC, Glaz MS, Ginger DS, Jen AKY. *Adv Mater*, 2015, 27: 695–701
132 Jung JW, Chueh CC, Jen AKY. *Adv Mater*, 2015, 27: 7874–7880
133 Kim J, Lee HR, Kim HP, Lin T, Kanwat A, Mohd Yusoff ARB, Jang J. *Nanoscale*, 2016, 8: 9284–9292
134 Chen W, Wu Y, Yue Y, Liu J, Zhang W, Yang X, Chen H, Bi E, Ashraful I, Grätzel M, Han L. *Science*, 2015, 350: 944–948
135 Rao H, Ye S, Sun W, Yan W, Li Y, Peng H, Liu Z, Bian Z, Li Y, Huang C. *Nano Energy*, 2016, 27: 51–57
136 Li Z. *Chem Lett*, 2015, 44: 1140–1141
137 Chen W, Wu Y, Liu J, Qin C, Yang X, Islam A, Cheng YB, Han L. *Energy Environ Sci*, 2015, 8: 629–640
138 Shen W, Yang C, Bao X, Sun L, Wang N, Tang J, Chen W, Yang R. *Mater Sci Eng-B*, 2015, 200: 1–8
139 Yu W, Li F, Wang H, Alarousu E, Chen Y, Lin B, Wang L, Hedhili MN, Li Y, Wu K, Wang X, Mohammed OF, Wu T. *Nanoscale*, 2016, 8: 6173–6179
140 Zhang H, Wang H, Chen W, Jen AKY. *Adv Mater*, 2017, 29: 1604984
141 Hones P, Diserens M, Lévy F. *Surf Coat Tech*, 1999, 120–121: 277–283
142 Wang M, Tang Q, An J, Xie F, Chen J, Zheng S, Wong KY, Miao Q, Xu J. *ACS Appl Mater Interfaces*, 2010, 2: 2699–2702
143 Liu Z, Seo S, Lee EC. *Appl Phys Lett*, 2013, 103: 133306
144 Irfan , Zhang M, Ding H, Tang CW, Gao Y. *Org Electron*, 2011, 12: 1588–1593
145 Sweetnam S, Graham KR, Ngongang Ndjawa GO, Heumüller T, Bartelt JA, Burke TM, Li W, You W, Amassian A, McGehee MD. *J Am Chem Soc*, 2014, 136: 14078–14088
146 Tao C, Ruan S, Xie G, Kong X, Shen L, Meng F, Liu C, Zhang X, Dong W, Chen W. *Appl Phys Lett*, 2009, 94: 043311
147 Qiu M, Zhu D, Bao X, Wang J, Wang X, Yang R. *J Mater Chem A*, 2016, 4: 894–900
148 Hutter OS, Hatton RA. *Adv Mater*, 2015, 27: 326–331
149 Wang HQ, Li N, Guldal NS, Brabec CJ. *Org Electron*, 2012, 13: 3014–3021
150 Gong C, Yang HB, Song QL, Li CM. *Org Electron*, 2012, 13: 7–12
151 Guo CX, Sun K, Ouyang J, Lu X. *Chem Mater*, 2015, 27: 5813–5819
152 Park MH, Li JH, Kumar A, Li G, Yang Y. *Adv Funct Mater*, 2009, 19: 1241
153 Li XC, Xie FX, Zhang SQ, Hou JH, Choy WCH. *Light: Sci Appl*, 2015, 4: e273